Incorporation of strontium-containing bioactive particles into PEOT/PBT electrospun scaffolds for bone tissue regeneration

Biomaterials Advances 149 (2023) 213406

Contents lists available at ScienceDirect

Biomaterials Advances

journal homepage: www.journals.elsevier.com/materials-science-and-engineering-c

Incorporation of strontium-containing bioactive particles into PEOT/PBT electrospun scaffolds for bone tissue regeneration

Clarissa Tomasina [a], Giorgia Montalbano [b], Sonia Fiorilli [b], Paulo Quadros [c], António Azevedo [c], Catarina Coelho [c], Chiara Vitale-Brovarone [b], Sandra Camarero-Espinosa [a,d,e], Lorenzo Moroni [a,*]

[a] MERLN Institute for Technology-Inspired Regenerative Medicine, Maastricht University, Complex Tissue Regeneration Department, Maastricht, the Netherlands
[b] Department of Applied Science and Technology, Politecnico di Torino, Torino, Italy
[c] FLUIDINOVA S.A, Rua de Rosa Jácome Felgueiras 57, Maia, Portugal
[d] POLYMAT, University of the Basque Country, UPV/EHU, Avenida Tolosa 72, Donostia 20018, Gipuzkoa, Spain
[e] IKERBASQUE, Basque Foundation for Science, 48009 Bilbao, Spain

ARTICLE INFO

Keywords:
Hydroxyapatite
Bioactive glasses
Strontium
Electrospinning
Bone
Human mesenchymal stem cells

ABSTRACT

The combination of biomaterials and bioactive particles has shown to be a successful strategy to fabricate electrospun scaffolds for bone tissue engineering. Among the range of bioactive particles, hydroxyapatite and mesoporous bioactive glasses (MBGs) have been widely used for their osteoconductive and osteoinductive properties. Yet, the comparison between the chemical and mechanical characteristics as well as the biological performances of these particle-containing scaffolds have been characterized to a limited extent. In this work, we fabricated PEOT/PBT-based composite scaffolds incorporating either nanohydroxyapatite (nHA), strontium-containing nanohydroxyapatite (nHA_Sr) or MBGs doped with strontium ions up to 15 wt./vol% and 12,5 wt./vol% for nHA and MBG, respectively. The composite scaffolds presented a homogeneous particle distribution. Morphological, chemical and mechanical analysis revealed that the introduction of particles into the electrospun meshes caused a decrease in the fiber diameter and mechanical properties, yet maintaining the hydrophilic nature of the scaffolds. The Sr^{2+} release profile differed according to the considered system, observing a 35-day slowly decreasing release from strontium-containing nHA scaffolds, whereas MBG-based scaffolds showed a strong burst release in the first week. *In vitro*, culture of human bone marrow-derived mesenchymal stromal cells (hMSCs) on composite scaffolds demonstrated excellent cell adhesion and proliferation. In maintenance and osteogenic media, all composite scaffolds showed high mineralization as well as expression of Col I and OCN compared to PEOT/PBT scaffolds, suggesting their ability to boost bone formation even without osteogenic factors. The presence of strontium led to an increase in collagen secretion and matrix mineralization in osteogenic medium, while gene expression analysis showed that hMSCs cultured on nHA-based scaffolds had a higher expression of OCN, ALP and RUNX2 compared to cells cultured on nHA_Sr scaffolds in osteogenic medium. Yet, cells cultured on MBGs-based scaffolds showed a higher gene expression of COL1, ALP, RUNX2 and BMP2 in osteogenic medium compared to nHA-based scaffolds, which is hypothesized to lead to high osteoinductivity in long term cultures.

1. Introduction

Bone tissue engineering aims at designing bone substitutes to repair the damaged or lost bone [1]. In fact, extensive studies have underlined the need to overcome the lack of bone donors and the limitations and drawbacks of the current standard clinical strategies such as allografts and autografts [2]. In the field of tissue engineering, the combination of cells, biomaterials and other bioactive agents is directed at enhancing the formation of neo-native bone tissue [3]. However, designing scaffolds requires a deep understanding of the tissue structure and composition as well as of the available manufacturing strategies to design biomimetic and bioactive constructs able to successfully promote regeneration.

In this context, biofabrication technologies enable control over the material deposition and the architecture of the final scaffold [4]. Of the various techniques, electrospinning certainly represents a promising

* Corresponding author.
E-mail address: l.moroni@maastrichtuniversity.nl (L. Moroni).

https://doi.org/10.1016/j.bioadv.2023.213406
Received 13 December 2022; Received in revised form 11 February 2023; Accepted 27 March 2023
Available online 29 March 2023

strategy to fabricate nanofibrous and porous scaffolds able to mimic the features of the native ECM [5]. In fact, electrospun scaffolds are formed by micrometer fibers that resemble the ECM as well as by micropores that ensure cell growth [6]. Microporosity can improve the attachment of bone-related cells by the generation of capillary-forces, can offer more protein adsorption sites thanks to the increased specific surface area and can accelerate the release of degradation products, which facilitate the interactions between scaffolds and cells [7]. The electrospinning process focuses on the formation and deposition of submicron fibers by the application of an electrostatic field on a polymer solution. Solution, process and environmental parameters can be tuned to alter the morphological feature of the final scaffold, while the physico-chemical properties will depend on the material of choice [8].

Amid the range of biocompatible materials, synthetic polymers have been commonly used in electrospinning and they offer a versatile tool since they are easily processed and functionalized [9]. In this frame, Polyactive© is a commercially available copolymer formed by poly (ethylene oxide terephthalate) (PEOT) and poly(butylene terephthalate) (PBT), which has been selected due to its biocompatibility, processability, mechanical properties and previous applicability in bone [10] and cartilage tissue engineering [11]. In fact, polyactive is also one of the few polymers to have shown rapid calcification and needle-shaped crystal within the surface in a calvarian envelope [12]. In addition, PEOT/PBT copolymers are biodegradable, showing around 17 wt% mass loss *in vitro* at 100 °C in phosphate buffer saline (PBS) during 14 days and only little degradation (under 5 wt% mass loss) after 6 months of implantation *in vivo* [13]. However, it is known that synthetic polymers alone are usually not sufficient to recreate the bone physical and chemical properties [14]. Therefore, particles or other bioactive molecules are commonly included in the fabrication process to better mimic bone composite structure and improve the bioactivity and biocompatibility of the bone scaffold [15].

Bone is formed by a dynamic matrix composed by mainly collagen I (COL1) and carbonated nanohydroxyapatite [1]. Hence, calcium phosphates such as hydroxyapatite (HA) partially resemble the native chemical composition and have been widely used in orthopedic applications to enhance the osteoinductive and osteoconductive properties of biomaterials [16]. In recent works, nanoHA has been incorporated into electrospun poly(lactic acid) (PLA) scaffolds in concentrations up to 20 wt% showing how 10 wt% HA was optimal to promote the expression of COL-I and BMP-2 osteogenic-related genes [17]. Similarly, HA was combined with poly(ε-caprolactone) (PCL) for MC-3 T3 cell culture where HA improved proliferation and ALP activity of cells [18].

Beside HA, mesoporous bioactive glasses (MBGs) are suitable candidates to promote bone formation and tissue healing [19] thanks to their high bioactivity, osteoconductivity and degradation rate [20]. Furthermore, these inorganic phases are characterized by a mesoporous structure, large pore volume and high exposed surface area [21]. In a recent work [22], MBGs were incorporated into poly(caprolactone-*co*-glycolide) (PGA-PCL) electrospun scaffolds showing how the addition of inorganic phases could improve the hydrophilicity and apatite-formation ability, as well as the osteogenic capacity of the scaffolds. To further improve the biomaterial to cell interaction, MBGs can be easily enriched with functional groups such as amino groups [23] as well as doped with specific elements such as zinc [24] and copper [25].

Among the therapeutic ions suitable for bone regeneration, strontium has been widely used for its influence on bone cells [26]. This element was shown to improve bone formation by increasing osteoblasts activity while hindering the growth of osteoclasts and reducing bone resorption [27]. Ye et al. [28] showed that strontium-substituted hydroxyapatite could be incorporated into PCL/chitosan scaffolds giving rise to a sustained release of strontium and promoting rat BMSCs adhesion, proliferation and ALP activity. In another study [29], strontium-doped borosilicate bioactive glasses were included into PLA to form fibrous scaffolds where they were able to promote ALP, SP7 and OCN gene expression in hMSCs.

Despite the incorporation of strontium-containing HA and MBGs into electrospun scaffolds has been already reported, composite scaffolds made of Polyactive (PEOT/PBT) and nHA or MBGs were never fabricated and investigated in terms of fiber morphology and chemically and mechanically properties. In addition, there is a lack of data comparing the effect of these composite scaffolds on hMSCs differentiation towards an osteogenic phenotype in long term cultures looking also at collagen secretion and gene expression of more mature bone markers such as BMP2. In this study, we fabricated PEOT/PBT composite scaffolds by incorporating bioactive particles in the electrospinning process. Composites were prepared by the incorporation of either nano-hydroxyapatite particles (nHA) with (nHA_Sr) or without strontium or strontium-doped mesoporous bioactive glasses fabricated through sol-gel (MBG_SG) and spray-drying (MBG_SD) techniques. The kinetics of ion release from the inorganic phases was evaluated during the different steps of the fabrication process as well as after incorporation into the polymeric mesh to ensure particle functionality. Upon fabrication, electrospun composite scaffolds were morphologically, chemically and mechanically characterized. The bioactive composite scaffolds performances were also compared in *in vitro* long-term culture of hMSCs (35 days) in terms of collagen secretion, protein expression, extracellular matrix (ECM) production and mineralization, and gene expression.

2. Material and methods

2.1. Materials

2.1.1. Synthesis of inorganic phases

nHA-based particles were provided by FLUIDINOVA S.A and were synthetized using a NETmix reactor containing aqueous solutions of Ca^{2+} and $PO4^{3-}$ [30,31]. For the 50 % calcium substitution, after implementing an additional source for strontium, samples underwent wet chemical precipitation and were further washed to remove residual ions. Finally, samples were concentrated in a suspension of 15,5 ± 1.0 wt%.

Strontium enriched MBGs were synthetized following protocols previously optimized and reported by the authors [32]. Two different synthesis methods were exploited to produce micro and nano-sized spherical particles of MBG containing a final 10 % molar strontium concentration. In brief, an aerosol-assisted spray-drying approach was used to produce micro-sized MBGs (MBG_SD), while nanoparticles of MBG (MBG_SG) were obtained exploiting a base-catalysed sol–gel synthesis. Experimental details about the two different synthesis methods used to produce MBG particles are reported in the Supplementary Information.

2.2. Particle characterization

2.2.1. Transmission electron microscopy

Particles were added at a 5 wt./vol% in chloroform and sonicated using a horn sonicator (50 % amplitude, frequency 20 kHz, SONOPULS HD 2000.2, Bandelin) for different time points (5 min and 7 min). After sonication, samples were left air dry overnight and then re-dispersed in absolute ethanol. A 10 μl droplet of particle suspension was then deposited on top of a copper grid, then tilted to eliminate the ethanol in excess and let air dry. Finally, samples were imaged using a FEI Tecnai G2 Spirit BioTWIN iCorr microscope.

2.2.2. Strontium release

Particles were dispersed at 5 wt./vol% in chloroform and the strontium release was monitored after sonication for 5 min and after the final addition of 1,1,1,3,3,3-hexafluoro-2-propanol (HFIP). Since HFIP is a component of the solvent mixture used for scaffold fabrication, it was added at a later stage to investigate if it affected the strontium content in the particles. The particles collected at the different processing steps, were firstly air dried overnight and then dissolved in a mixture of nitric

and hydrofluoric acids and subsequently analyzed, via Inductively Coupled Plasma Atomic Emission Spectrometry Technique (ICP-AES) (ICP-MS, Thermoscientific, Waltham, MA, USA, ICAP Q), in order to calculate the final percentage of the released ions on the basis of the measured concentration values (expressed as ppm). The percentage of ion released was calculated by considering the amount of strontium initially incorporated in the inorganic particles, obtained by performing the same analysis on untreated samples.

2.3. Scaffold fabrication

For the fabrication of scaffolds, poly(ethylene oxide terephthalate)/poly(butylene terephthalate) (PEOT/PBT) was supplied by PolyVation (the Netherlands). Traditional electrospinning was performed using 300PEOT55PBT45, being 300 (Mw, g/mol) the molecular weight of the initial PEG segments for polymerization and 55 and 45 the weight ratio of PEOT and PBT, respectively. PEOT/PBT was dissolved at 28 wt./vol% in a mixture of chloroform (anhydrous, Sigma-Aldrich) and HFIP (BioSolve B·V) ($CHCl_3$:HFIP) (75:25) overnight. For composite scaffolds, particles were sonicated in chloroform and added to the PEOT/PBT solution. After 1 h of stirring, the resulting solution was used for the spinning process. For that, the polymer flow was set at 0.12 ml/h and the jet was spun at 20 kV through a 0.8 mm spinneret at a distance of 12 cm from the collector and at a temperature of 25 °C and humidity of 35 %. To optimize the particle concentration and distribution in the electrospun meshes, particle concentrations ranging from 5 wt./vol% to 15 wt./vol% were explored and composite formulations were spun on a flat stainless steel collector with a spinning time of 15 min. For the production of scaffolds for in vitro characterization, a polypropylene sheet was punched using a 12 mm puncher to create a hollow sheet that was mounted on a rotating mandrel. The mandrel was used as a collector at 1500 rpm and the spinneret was moved along the mandrel during the fabrication. Samples obtained from the hollow sheet were further punched concentrically to the holes using a 15 mm puncher, creating a sample supported by a polypropylene ring.

2.4. Morphological and chemical characterization

2.4.1. Scanning electron microscopy (SEM) and energy dispersive X-ray (EDX) analysis

For the characterization of the fiber diameter, mesh morphology and particle distribution, electrospun scaffolds were mounted on aluminum pin stubs with the use of carbon tape and later gold coated using a Cressington Sputter Coated 180 auto and imaged using a Jeol JSM-IT200 InTouchScope scanning electron microscope operating at 10 keV. Fiber diameter was calculated by selecting 25 fibers from 4 different images in the meshes using Fiji Software. Similarly, samples were quickly cooled with liquid nitrogen, cut in the middle and mounted onto a 90° degree angled pin stub (Electron Microscopy Science) for calculation of scaffold thickness through SEM. In addition, for the analysis of the scaffold composition, samples were studied under the energy dispersive X-ray analyzer (EDX) coupled to the Jeol JSM-IT200 microscope.

2.4.2. Transmission electron microscopy (TEM)

Electrospun scaffolds with nHA and nHA_Sr were embedded in Epon 112© epoxy resin for 72 h at 60 °C. Then, a LEICA EM UC7 ultra microtome equipped with a diamond knife was used to cut ultrathin 50 nm sections. Finally, sections were recovered from water, placed on a carbon coated copper TEM grid and imaged with a FEI Tecnai G2 Spirit BioTWIN iCorr microscope.

2.4.3. Fourier transform infrared spectroscopy

Attenuated total reflectance-Fourier-transform-infrared (ATR-FTIR) spectroscopy was performed on electrospun scaffolds using a Nicolet iS50 in the 4000–400 cm^{-1} range with accumulation of 32 scans. Furthermore, to confirm the presence of particles embedded in the matrix, chemical structure characterization was also performed on particles powders.

2.4.4. Contact angle

Wettability of scaffolds was determined by measuring the static contact angle by means of the sessile drop technique. Briefly, 4 μl of distilled water were deposited on the surface of electrospun scaffolds in triplicate samples and measurements were recorded using an optical contact angle device DSA25 (KRÜSS GmbH) equipped with an electronic syringe unit (OCA15, Dataphysics, Germany).

2.5. Mechanical characterization

To investigate the influence of particles on the mechanical properties of PEOT/PBT electrospun scaffolds, tensile tests were performed using a mechanical tester (ElectroForce 3200, TA Instruments) equipped with a 4,5 N load cell and controlled with Wint7 software. Samples were mounted using paper strips attached to the sample extremes using adhesive glue (Loctite 431, Farnell). The strips were inserted into the gripping equipment to hold the sample, leaving only the electrospun mesh secured between the grips. Sample dimensions were then measured with a caliper and tested at a strain rate of 1 % strain/s at room temperature (RT). All scaffolds were measured in dry state until creep (or until maximum load). The Young's modulus was calculated from the elastic region (0.02–0.1 strain) of stress-strain curves and the ultimate tensile strength was taken from the highest stress point before sample creep from the stress-strain curve.

2.6. Strontium release from composite scaffolds

PEOT/PBT-based scaffolds of 15 mm diameter were detached from the aluminum support used for spinning and placed in 24-well plates. After been secured with an O-ring (Eriks), samples were sterilized for 15 min with ethanol and let air dry overnight. Afterwards, samples were incubated with PBS over a period of 35 days. PBS was changed and collected after 12 h to resemble the pre-wetting step of scaffolds and then every other day. Upon collection of the medium at the different time points considered, the concentrations of strontium ions were measured by ICP-MS.

2.7. hBMSCs culture and differentiation

HMSCs were purchased from Lonza (Donor 36,550, male, age 25). Cells were cultured at a density of 1000 cells/cm^2 in α-MEM (minimum essential medium) (Gibco) supplemented with 10 % FBS (Fetal Bovine Serum) (Sigma-Aldrich). Cells were passaged at 70–80 % confluency and used at passage 5 for all experiments.

2.7.1. Cell culture in 2D

As a control, hMSCs were seeded in 6-well plates at a density of 5000 cells/cm^2 and were cultured in α-MEM with 10 % FBS and 100 U/ml penicillin-streptomycin (Sigma-Aldrich) (maintenance medium) for 7 days until reach confluency. Afterwards, maintenance medium was continued or replaced with alpha-MEM with 10 % FBS, 0.2 mM L-ascorbic acid-2-phosphate (Sigma-Aldrich), 10 nM dexamethasone (Sigma-Aldrich), 10 mM β-glycerophosphate (Sigma-Aldrich) and 100 U/ml penicillin-streptomycin for 4 weeks (osteogenic medium).

2.7.2. Cell culture on electrospun scaffolds

Electrospun scaffolds were obtained using a 15 mm puncher and placed in a 24-well plate after being detached from the aluminum foil. On top of the scaffolds, O-rings were used to secure the scaffold to the bottom of the well. Scaffolds were then sterilized with 70 % ethanol for 30 min and let it air dry overnight. Afterwards, scaffolds were pre-wetted using α-MEM supplemented with 100 U/ml penicillin-streptomycin for 12 h at 37 °C before seeding.

HMSCs were seeded at passage 5 at a density of 50,000 cells/cm^2 and cultured for 7 days in maintenance medium. After a week of proliferation (day 0), medium was replaced to osteogenic medium for 4 weeks of differentiation (day 28).

2.7.3. hMSCs viability and proliferation

2.7.3.1. Live/dead assay. 24 h after seeding, a viability assay was performed using live/dead Fixable Far-Red Dead Cell Stain Kit for 633 or 650 nm excitation wavelength (L34973, Thermo Fisher). Briefly, scaffolds were washed twice with PBS and incubated with the far-red fluorescent reactive dye (0,5 μl dye in 500 μl PBS) for 30 min in the dark at RT. The samples were then washed with PBS, fixed with 4 % paraformaldehyde (PFA) (Sigma-Aldrich) for 20 min and permeabilized with 0,1 % triton X-100 (Sigma-Aldrich) for 15 min. To reduce the background autofluorescence, scaffolds were stained with 0,1 % Sudan Black (Sigma-Aldrich) in 70 % ethanol for 45 min and then washed with PBS. Finally, samples were incubated in Hoechst 33342 (1:1000) (Thermo Fisher) in PBS for 10 min and in Alexa Fluor 568 Phalloidin (1:100, Thermo Fisher) for 45 min and imaged using an Nikon Ti-E microscope, equipped with a Lumencor Spectra light source, an Andor Zyla 5.5 sCMOS camera, and an MCL NANO Z200-N TI z-stage.

2.7.3.2. DNA assay. After 1 week of proliferation, scaffolds were washed with PBS, removed from the support and moved to Eppendorf tubes at −80 °C. Then, scaffolds underwent three cycles of thawing at RT and freezing at −80 °C to facilitate the lysis of the cells. To digest the extracellular matrix, scaffolds were incubated overnight at 56 °C with 250 μl of 1 mg/mL proteinase K (Sigma-Aldrich) in a 50 mM Tris/1 mM ethylenediaminetetraacetic acid/1 mM iodoacetamide solution. After overnight incubation, three freeze-thawing cycles were repeated and the DNA Assay was performed using a CyQUANT™ Cell Proliferation Assay kit following manufacturer protocol. Briefly, scaffolds were incubated at RT in 250 μl of lysis buffer supplemented with DNAse-free RNase A (1:500) (Thermo Fisher) to eliminate the RNA component of the fluorescent signal. Finally, 100 μl of each sample were transferred to a 96-well plate in triplicate together with 100 μl of a 2× GR-dye solution and incubated for 10 min at RT. A DNA standard was used to create a standard curve and fluorescent intensity was measured at 520 nm using a CLARIOstar spectrophotometer.

2.7.4. Collagen secretion

Collagen (I and III) secretion in medium was analyzed at day 14 and day 28 following a previous published protocol [33]. Culture medium was refreshed two days prior the time-point with the corresponding medium without FBS in order to avoid background signal. Briefly, 1 ml of culture medium was mixed with 1 ml of 0,1 % Sirius Red dye (Sigma-Aldrich) solution in 0,5 M acetic acid (Sigma-Aldrich) for 30 min at 4 °C. Samples were then centrifuged at 15000 *g* for 20 min at 4 °C and pellets were washed twice with 0,5 M acetic acid. Lastly, samples were dissolved in 1 ml of 0,5 M NaOH and 100 μl of each samples were pipetted in triplicate in a 96-well plate and measured at 530 nm using a CLARIOstar spectrophotometer. Collagen I solution (Cell Systems) was used to generate a standard curve.

2.7.5. Immunofluorescence

Scaffolds were fixed with 4 % PFA at day 28 in maintenance and osteogenic medium, followed by rinsing with PBS and permeabilization for 30 min with 0,1 % Triton X-100. Then, scaffolds were stained with 0,1 % sudan black in 70 % ethanol for 45 min and washed with PBS until the solution was clear. Blocking was done for 1 h in 1 % Bovine Serum Albumin (VWR), 5 % goat serum (Sigma-Aldrich) and 0,05 % Tween-20 in PBS. Samples were then incubated in mouse anti-collagen I (1:100, ab6308 Abcam) and rabbit anti-osteocalcin (1:100, ab93876 Abcam) overnight at 4 °C. After incubation, primary antibodies were washed with PBS. Secondary antibodies (goat anti-mouse and goat anti-rabbit, 1:300, Abcam) and Alexa Fluor Phalloidin 647 (1:100, Thermo Fisher) in PBS were added to the samples and then left in the dark for 45 min at room temperature. Samples were further stained for DNA with Hoechst 33342 (1:1000) in PBS for 15 min and rinsed with PBS. Last, samples were mounted with DAKO mounting medium on a glass slide and imaged using a Leica TCS SP8 CARS confocal microscope.

2.7.6. ECM mineralization assay

Alizarin Red staining (ARS) was used to qualitatively observe the calcium deposits on the scaffolds. At day 28, scaffolds were fixed with 4 % PFA for 30 min and washed with distilled water. An Alizarin red solution (40 mM, ph 4.1–4.3) was prepared in distilled water and applied on scaffolds for 20 min at RT. After incubation, scaffolds were washed with distilled water overnight. For quantification of the dye, samples were detached from the support and placed in a Eppendorf with 400 μl of 10 % chloride monohydrate (CPC) in 10 mM sodium phosphate (ph 7) overnight. Once the dye was completely extracted, 100 μl of each sample were measured in triplicates in a 96-well plate at 562 nm using a CLARIOstar spectrophotometer. A standard curve was performed using a dilution series of alizarin red solution in 10 % CPC. Bare scaffolds were used as a control.

2.7.7. ECM morphology

At day 28, scaffolds were imaged using SEM. First, scaffolds were fixed with 4 % PFA for 30 min, followed by rinsing three times with PBS. Then, scaffolds were dehydrated using a series of ethanol dilutions (30, 50, 70, 80, 90, 96 and 100 % in water for 15 min) at RT. Finally, samples were incubated in pure ethanol: hexamethyldisilazane (HMDS) (50:50) for 15 min and additionally in HMDS for 15 min, followed by overnight air drying at RT after removal of the HMDS. Samples were gold sputter coated as described previously and imaged using a Jeol JSM-IT200 InTouchScope at 10 kV.

2.7.8. Gene expression

To investigate the gene expression at day 28, RNA was extracted from samples using a RNeasy mini kit (Qiagen) with a Trizol digestion step. In brief, scaffolds were washed with PBS, detached from the support and placed in 1 ml of Trizol in triplicates. Samples were then centrifuged at 12000 *g* for 5 min at 4 °C to precipitate the ECM and 200 μl of chloroform were further added to each sample. After centrifugation at 12000 *g* for 15 min, the aqueous phase was recovered and the DNA purified using RNeasy mini kit column (Qiagen) following suppliers protocol. Concentration and purity of RNA were measured using a Spectramax QuickDrop Micro-Volume spectrophotometer. cDNA was synthetized using iScript cDNA synthesis kit (Bio-Rad) following manufacturer's instructions. Finally, qPCR reactions were conducted in 20 μl total volume mixing 3 ng of cDNA, 0,2 uM of selected primers (Table S1) and SYBR Green Supermix (Qiagen). A CFX Connect Real-Time System (Bio-Rad) was used with the following thermal cycle: 95 °C for 3 min, 40 cycles for 15 s at 95 °C and 30s at 55 °C. For each target gene, B2M was selected as housekeeping gene for normalization and the $2^{-\Delta\Delta Ct}$ method was performed to calculate the relative expression. Further normalization was done with reference to the relative expression of cells cultured on the PEOT/PBT scaffolds in maintenance or osteogenic medium. For hBMSCs culture in 2D, gene expression in maintenance medium was used for normalization.

2.8. Statistical analysis

All data is expressed as mean ± standard deviation and the number of replicates (n) is reported in the figure captions. For Young's modulus, DNA Assay, collagen secretion, alizarin red and qPCR, statistical significance was calculated with GraphPad Prism 8 (GraphPad Prism Software) using a one-way analysis of variance (ANOVA) with Tukey's multiple comparison test: n.s $p > 0.05$, (****) $p < 0.0001$, (***) $p <$

0.001, (**) $p < 0.01$, and (*) $p < 0.05$.

3. Results

3.1. Particle characterization

To improve particle distribution into the PEOT/PBT solution, nHA, nHA_Sr and MBG_SG and MBG_SD particles were separately sonicated using a horn sonicator prior introduction into the polymeric solution and consequent fabrication by electrospinning (Fig. 1, A). As stated in previous studies [32], textural and morphological analysis revealed that the size of MBG_SG particles was in the range 200–500 nm and their specific surface area was 465 m^2/g, with average pore of 4 nm and pore volume of 0.33 cm^3/g, whereas for MBG_SD particles size was in the range of 500 nm-2 μm and they had a surface area of 85 m^2/g with 7–11 nm pores of 0.23 cm^3/g volumes. nHA particles were previously characterized to have an average size of 66 nm with a Ca/P molar ratio of 1,68 ± 0,03 [30]. To evaluate the potential effect of the electrospinning solvent (e.g. chloroform and HFIP (75:25)) on particle aggregation and the effects of sonication on particle integrity and dispersibility, the morphology of the different inorganic phases was evaluated using TEM (Fig. S1). Before sonication, nHA particles were observed as big aggregates composed of small nanorods of around 50 nm each. After 5 min of sonication, the particles disaggregated substantially with clump sizes of approximately 200 nm whereas no morphology changes were observed. Based on this, and to avoid potential ion release due to the sonication steps, shorter sonication times were preferred for both nHA_Sr and nHA. In the case of MBG particles, the TEM images revealed the presence of particles fragments after 7 min of sonication. Same as for nHA, 5 min of sonication were selected to preserve the strontium content and still allow for a better dispersion of particles in the solvent (Fig. 1B).

To further investigate the particle stability during the fabrication process, ion release from strontium-containing particles was evaluated after sonication and after incubation in the electrospinning solvent (Fig. 1C), where untreated nHA particles were adopted as control establishing a no strontium release background during the process. nHA_Sr had a percentage of Sr^{2+} of 34,1 %, which decreased to 32,3 ± 1,1 % after sonication and further to 28,9 ± 1,2 % after incubation. Similarly, Sr^{2+} release from MBGs was investigated for MBG_SD and MBG_SG particles. Both MBGs showed no significant change in the percentage of Sr^{2+} after the sonication and incubation steps with values that remained invariable at around 12 % and 9 %, respectively.

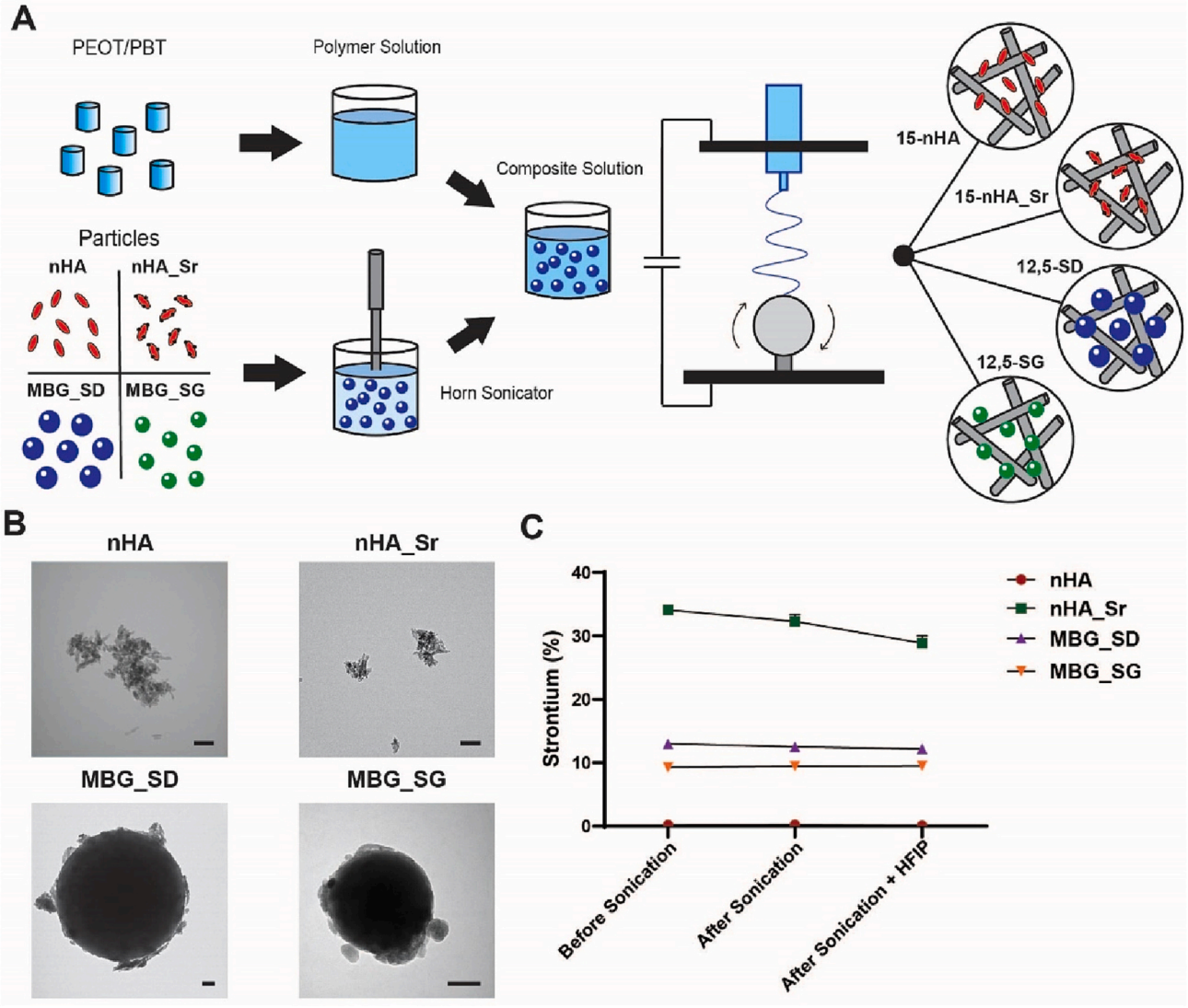

Fig. 1. Schematics of the particle incorporation process (A), TEM of the particles after sonication (B) and strontium release before and after sonication and further incubation in HFIP (C). Scale bar (B) is 100 nm.

3.2. Scaffold fabrication, chemical composition and mechanical properties

To fabricate composite scaffolds, different particle concentrations ranging from 5 wt./vol% to 15 wt./vol% were incorporated into PEOT/PBT scaffolds (Fig. S2). No particle sedimentation was observed in the electrospinning solution during fabrication. As shown in Fig. 2, it was possible to incorporate up to 15 wt./vol% nHA (15-nHA) and 15 wt./vol % nHA_Sr (15-nHA_Sr) while MBGs were included up to 12,5 wt./vol%, for both MBG_SD (12,5-SD) and MBG_SG (12,5-SG) particles. Regardless of the inorganic phase considered, all composite scaffolds were characterized by a porous structure, random fiber orientation and bead-free morphology. Fiber diameter was in the range of 1,06 ± 0,11 μm for PEOT/PBT and around 0,67 ± 0,14 μm for 15-nHA. No significant difference was observed between 15-nHA and 15-nHA_Sr (0,68 ± 0,15 μm) in terms of fiber dimension. For MBGs, an average fiber diameter of 0,59 ± 0,25 μm and 0,76 ± 0,27 μm was recorded for 12,5-SD and 12,5-SG, respectively. In addition, for all the composite meshes, particles looked distributed throughout the mesh showing small aggregates of around 10 μm in size.

To explore the particle distribution into the electrospun meshes, the interior structure of nHA-containing fibers was examined by TEM. Considering the small size of nHA particles compared to the fiber diameter, it was hypothesized that a part of the incorporated nHA would be embedded into the PEOT/PBT fibers. As shown in Fig. S3 (A), nHA particles were found inside the fiber structure when included at 5 wt./vol% up to 15 wt./vol%. Likewise, 15-nHA_Sr exhibited the same structure (Fig. S3, B). The presence of particles in the interior structure of fibers could affect the final properties of the scaffolds such as mechanical properties and ion release.

Beside exploring the fiber cross-section, membrane cross-section was also imaged through SEM (Fig. S4), measuring an average thickness of about 156,4 ± 35,3 μm for all composites. This result was expected and is aligned with the used spinning time (e.g.1 h and 30 min for all the formulation tested).

FTIR analysis was performed to further confirm the presence of the particles into the scaffolds. All composite scaffolds showed the typical bands associated with PEOT/PBT (Fig. S5) [34]. The CH_2 symmetric and asymmetric vibration stretches were located at 2868 cm^{-1} and 2956 cm^{-1}, respectively. Furthermore, it was possible to identify the C═O stretch mode at 1711 cm^{-1} and the C—O stretch mode at 1266 cm^{-1}. Last, the C-O-C stretching of the ether was observed at 1100 cm^{-1} while the aromatic C—H at 726 cm^{-1}.

As expected, the spectrum collected from 15-nHA and 15-nHA_Sr scaffolds showed the characteristic bands associated to hydroxyapatite [35] (Fig. 3A). The O—H vibration mode was observed at 630 cm^{-1} while the $(PO_4)^{3-}$ bands were located at 473 cm-1, 560 cm^{-1}, 600 cm^{-1} and 1023 cm^{-1}. Interestingly, the FTIR spectra of nHA_Sr and 15-nHA_Sr did not present the O—H band, suggesting the strontium incorporation into the particle framework. In the case of 12,5-SD and 12,5-SG scaffolds, the spectra displayed the peaks related to MBGs. Considering that MBG particles differ only for structural features and present the same chemical composition, no significant difference was observed between the spectra of the corresponding composite scaffolds. In particular, the

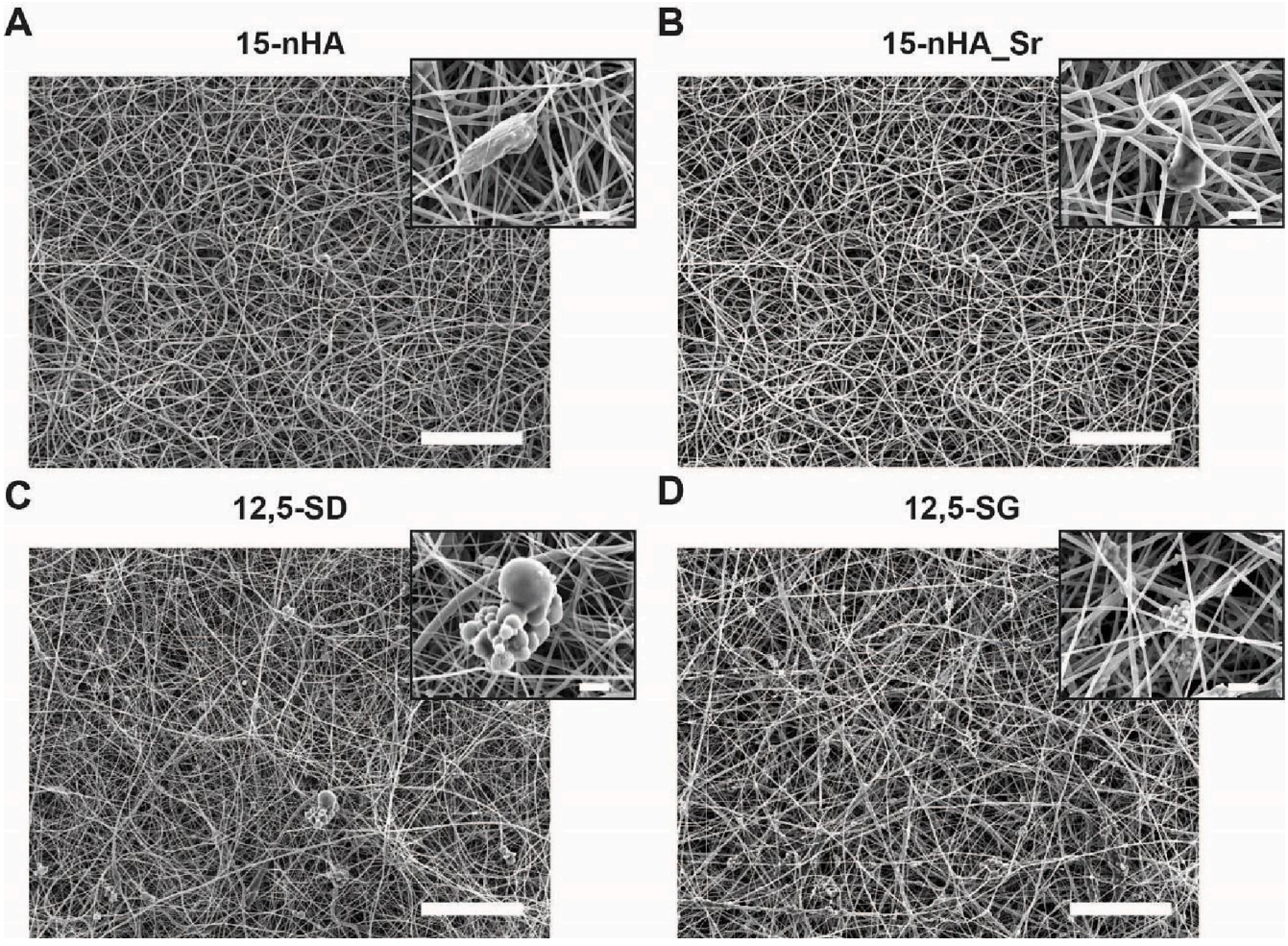

Fig. 2. Morphology of electrospun composite scaffolds. SEM images of composite electrospun scaffolds: 15-nHA (A), 15-nHA_Sr (B), 12,5-SD (C) and 12,5-SG (D). Top inserts show a zoom-in of the particles embedded in the matrix. Scale bar is 50 μm (5 μm in inserts).

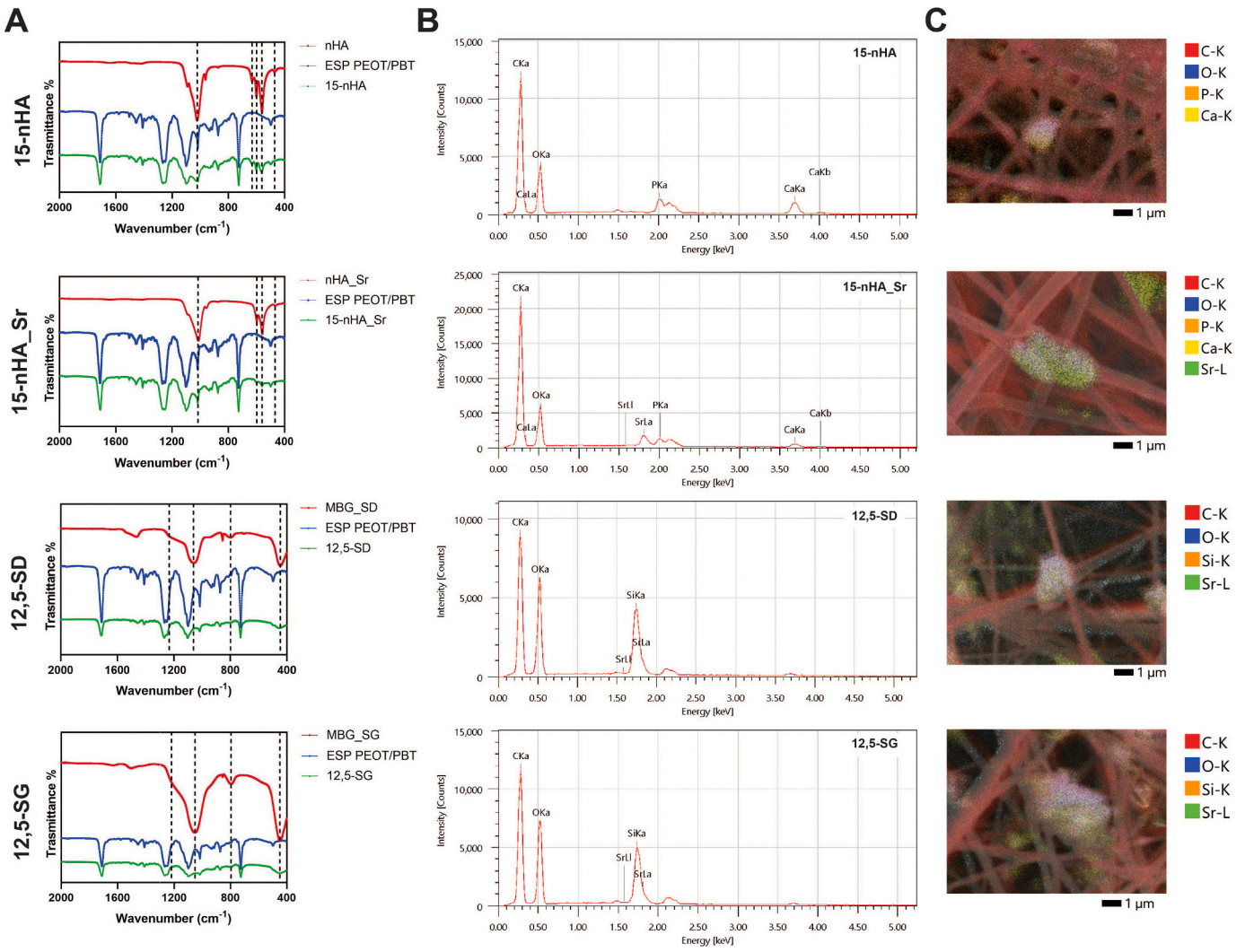

Fig. 3. Chemical composition of electrospun composite scaffolds. FTIR (A) and EDX (B) and maps of the elements (C) of composite scaffolds.

Si-O-Si bending was present at 447 cm^{-1} and the Si-O-Si symmetric and asymmetric stretching modes were located at 798 cm^{-1} and at 1058 cm^{-1} and 1244 cm^{-1}, respectively.

In addition, EDX analysis was used to specifically detect the presence of Ca, P, Si and Sr in the composite scaffolds containing HA or MBGs particles. As reported in Fig. 3 (B), EDX showed that 15-nHA scaffolds had a Ca/P ratio of 1,93, a similar value to those recorded for native bone tissue [36]. Similarly, 15-nHA_Sr showed a Ca/P of 1,27 and the inclusion of Sr was confirmed by the presence of a characteristic peak at 1,8 KeV. The lower Ca/P ratio of 15-nHA_Sr can be related to the synthesis process which involves the substitution of Ca with Sr, lowering the element concentration [37]. For MBG containing scaffolds, the presence of elements such as Sr and Si, according to the chemical composition of the glass, was confirmed also in the composite scaffolds. Mapping of elements (Fig. S6) corroborated the presence of Ca and P for nHA-containing scaffolds and Si and Sr for MBGs-containing scaffolds, respectively. Elements were segregated in the area where particles were deposited.

The wettability of the electrospun scaffolds was evaluated using contact angle measurement (Supplementary Videa S1-S5). On all scaffolds, the water drop rapidly penetrated into the mesh, indicating the hydrophilic properties of the material, even when particles were incorporated. Due to the rapid absorption of the water drop by the scaffolds and the dynamic character of the recorded videos, it was not possible to perform a quantitative measurement of the contact angle. Moreover, considering the rapid spreading of the water onto the scaffold surface within 30s of contact, it is suggested that all scaffolds are hydrophilic.

Finally, the mechanical properties of the scaffolds were investigated by performing a uniaxial tensile strength test (Fig. 4, A). The Young's modulus of PEOT/PBT-based scaffolds decreased once the particles were incorporated, probably because the particles disrupted the continuity of the polymer fibers, acting as defect points upon application of tensional loads. Despite PEOT/PBT having the highest modulus (6,21 ± 0,33 MPa), 15-nHA scaffolds registered the highest modulus among all composites (3,74 ± 0,18 MPa), probably due to the smallest size of the particles that in turn had a lower impact on the fiber continuity. Considering no difference was observed in the morphology and particle distribution of the nHA and nHA_Sr-loaded scaffolds, the mechanical properties of 15-nHA_Sr scaffolds are considered comparable to 15-nHA scaffolds. No statistical difference was observed between 12,5-SD and 12,5-SG scaffolds, which showed a modulus of 2,41 ± 0,25 MPa and 1,79 ± 0,53 MPa, respectively. Detailed observation of the stress-strain curves (Fig. 4, B) revealed that PEOT/PBT scaffolds displayed an ultimate tensile strength (UTS) of 1,17 ± 0,11 MPa while 15-nHA showed an UTS of 0,79 ± 0,03 MPa, followed by 12,5-SD and 12,5-SG with 0,50 ± 0,14 MPa and 0,40 ± 0,06 MPa, respectively. Compared to bone, which shows a tensile strength of 150 MPa [38], composites and bare PEOT/PBT showed a much lower modulus, which makes them suitable for non-load bearing applications. Thus, these scaffolds could be suitable

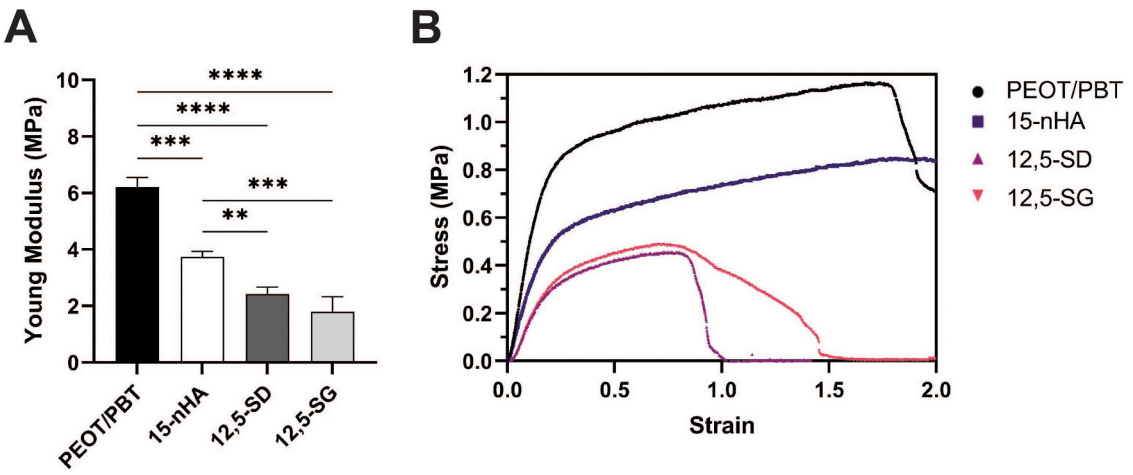

Fig. 4. Mechanical properties of electrospun composite scaffolds. Young's moduli of PEOT/PBT-based scaffolds (A) ($n = 3$) and representative stress-strain curves (B). For A, error bars represent mean ± SD and statistical significance was calculated using a one-way analysis of variance (ANOVA) with Tukey's multiple comparison test: n.s $p > 0.05$, (****) $p < 0.0001$, (***) $p < 0.001$, (**) $p < 0.01$, and (*) $p < 0.05$.

solutions for long flat bone fracture, such as the pelvis or the cranium where their flexibility could be of great advantage to be delivered by minimally invasive technique in the fracture site.

3.3. Sr^{2+} release profile from composite scaffolds

After fabrication of composite scaffolds, strontium release kinetics were investigated during a period of 35 days using ICP-MS (Fig. 5). PEOT/PBT and 15-nHA scaffolds were used as a control, confirming a negligible release of strontium from the meshes. As previously demonstrated, the optimized strategy used for the incorporation of particles into the electrospinning process allowed to preserve the particle ability to release ions. In fact, a burst release profile was observed for both MBGs in the first 3 days. This could be related to the very high porosity of MBGs, which makes them accessible to the medium and to the fast ion exchange reactions taking place on their surface [32]. It was observed that during the first 12 h, 12,5-SD and 12,5-SG had a release of 147,15 ± 16,67 ppm and 100,69 ± 5,35 ppm, respectively. Still, from day 3 to day 5 the Sr^{2+} release dropped to 8,59 ± 1,78 ppm for 12,5-SG and to 3,10 ± 0,77 ppm for 12,5-SD until reaching at day 35, 0,04 ± 0,01 ppm and 0,07 ± 0,01 ppm for 12,5-SG and 12,5-SD scaffolds, respectively. Considering that both MBGs were incorporated at 12,5 %, the higher Sr^{2+} values observed for 12,5-SG can be attributed to the higher molar percentage of strontium and the intrinsic properties of the particles. As a matter of fact, according to the ICP-MS (Fig. 1, C), the actual molar percentage of ion incorporation was around 12 % for MBG_SDs and 9 % for MBG_SGs. The higher strontium release from 15-SG compared to 15-SD could be related to the larger specific surface area and smaller pores that characterize MBG_SGs particles. 15-nHA_Sr showed a significantly lower Sr^{2+} release during the first days compared to the MBGs based scaffolds. However, from day 5, 15-nHA_Sr showed a higher and steady Sr^{2+} release compared to MBGs-based scaffolds starting at day 5 with 6,07 ± 0,60 ppm until day 35 with 3,74 ± 0,45 ppm.

3.4. Biocompatibility: hMSCs attachment and proliferation on electrospun scaffolds

The osteogenic potential of composite scaffolds was evaluated *in vitro* with the aim to investigate if nHA and MBGs particles, as well as the release of strontium ions, could boost bone formation compared to PEOT/PBT electrospun scaffolds.

Before evaluating the potential of the scaffolds to drive the formation of bone, their biocompatibility was assessed by adhesion and proliferation of hMSCs through evaluation of the cell viability after 1 week of culture.

Cell viability was evaluated with a live/dead assay, showing no

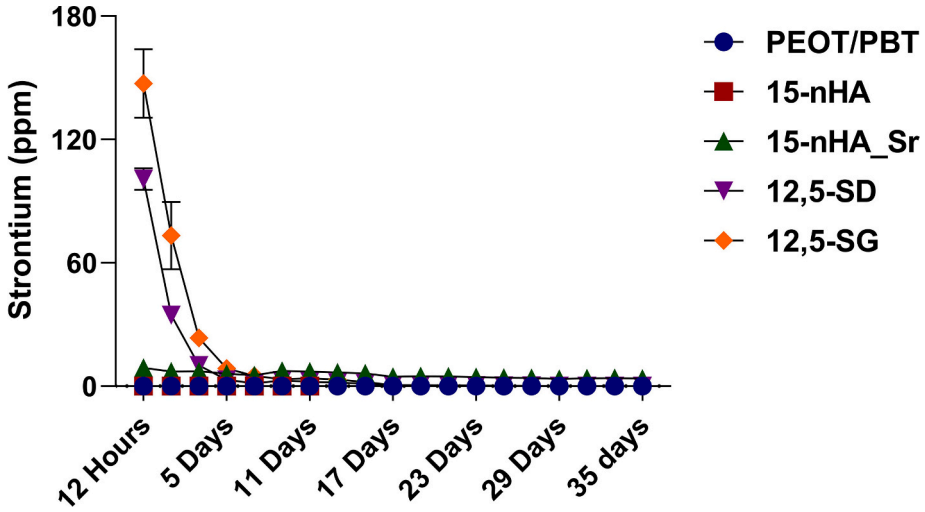

Fig. 5. Sr^{2+} release from composite scaffolds in PBS during a period of 35 days ($n = 4$). Error bars represents mean ± standard error.

significant number of dead cells in any of the tested conditions (Fig. 6, A). After 24 h of culture, cells adhered to all the scaffolds and spread on the surface. No significant difference was detected in the morphology of hMSCs, which appeared elongated and with a fibroblast-like morphology on all scaffolds. After confirming hMSCs attachment, cells were further cultured for 1 week and the cell number was quantified using a DNA assay (Fig. S7). After 1 week, no statistical difference was observed between the scaffolds. However, 12,5-SD and 12,5-SG showed a lower cell number compared to nHA and nHA_Sr-loaded scaffolds (126,817 ± 36,933 and 116,174 ± 8048 cells) and PEOT/PBT control (123,132 ± 13,414 cells), with 12,5-SG having 90,272 ± 17,090 cells and 12,5-SD being the lowest with 79,454 ± 11,417 cells, respectively.

3.5. Osteogenic differentiation on PEOT/PBT-based scaffolds

Afterwards, the capability of the scaffolds to promote osteogenic differentiation of hMSCs and the deposition of a mineralized bone matrix were evaluated. Collagen (I and III) secretion by hMSCs cultured on the different composite scaffolds was investigated at day 14 and 28 through Sirius red staining. At day 14, in maintenance medium (Fig. 6, B), 15-nHA_Sr showed the highest collagen secretion among composite scaffolds with 0,67 ± 0,09 mg/ml, which was also comparable to the amount of collagen secreted by hMSCs in 2D in the same medium (0,64 ± 0,07 mg/ml) (Fig. S8, C). Similarly, 12,5-SD and 12,5-SG scaffolds exhibited a higher collagen secretion (0,51 ± 0,03 mg/ml and 0,59 ± 0,04 mg/ml, respectively) compared to the PEOT/PBT control, but lower than in 15-nHA_Sr scaffolds. Only collagen secretion by hBMSCs on 15-nHA_Sr and 12,5-SG scaffolds resulted to be higher than that from 15-nHA scaffolds (0,34 ± 0,08 mg/ml). In osteogenic medium, collagen secretion was overall higher than in maintenance medium and cells cultured on 15-nHA_Sr scaffolds still displayed the highest collagen secretion (0,85 ± 0,07 mg/ml) compared to 15-nHA (0,54 ± 0,02 mg/ml) and PEOT/PBT (0,56 ± 0,09 mg/ml), followed by cells cultured in 12,5-SD collagen secretion (0,73 ± 0,07 mg/ml).

At day 28, collagen secretion increased in both maintenance and osteogenic medium (Fig. 6C). A similar increase was also observed in 2D cultures, where collagen secretion in maintenance medium (1,87 ± 0,10 mg/ml) was higher compared to osteogenic medium (0,90 ± 0,07 mg/ml). For scaffolds in maintenance medium, it was possible to observe the same trend as at 14 days with 15-nHA_Sr having a higher collagen secretion (1,37 ± 0,21 mg/ml) compared to the PEOT/PBT control. In osteogenic medium, all composite scaffolds containing strontium enabled higher collagen secretion compared to PEOT/PBT. These results were similar to what was observed in 2D where at day 28, BMSCs exhibited a similar collagen secretion of 0,9 ± 0,07 mg/ml. However, since values were not normalized to the DNA content, it was difficult to make a fair comparison between 2D and 3D cultures.

To assess the differentiation state of hMSCs at day 28, immunofluorescence was performed by staining the samples for OCN and COL1 in maintenance and osteogenic media (Fig. S9 and Fig. 7, A). In osteogenic medium, COL1 was present in all sample conditions alongside OCN. Interestingly, no difference was observed between the samples, which could be related to the high cell density on the scaffolds, as showed by F-actin staining. In addition, while OCN was found also in maintenance medium (Fig. S9), COL1 deposition in this medium was more pronounced, but appeared to be only intracellularly expressed. Similarly, the cells had a spindle morphology and were covering the whole scaffold surface.

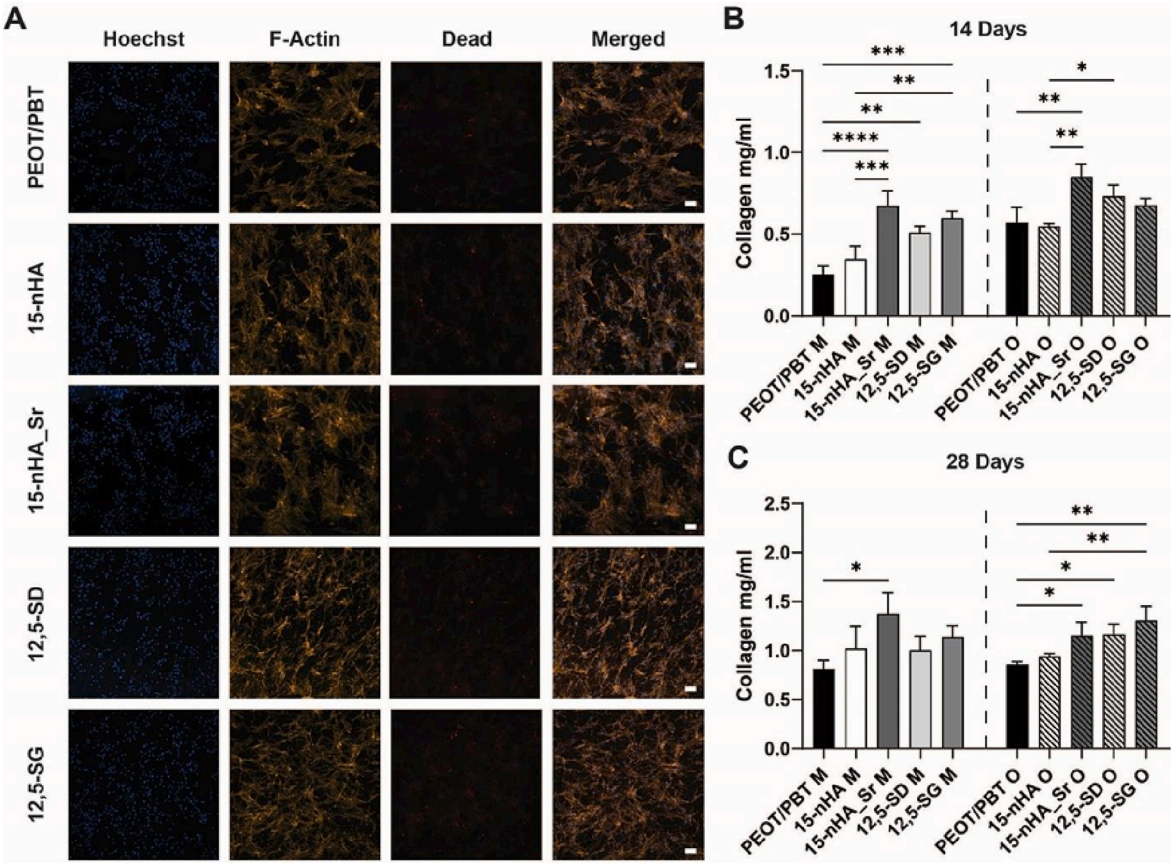

Fig. 6. Cell viability and collagen secretion. Fluorescence images of live/dead assay at 24 h after seeding (A). Cells were stained for DNA (blue, Hoechst), F-actin (orange, phalloidin) and propidium iodide (red). Scale bar is 100 μm. HMSCs collagen secretion in maintenance and osteogenic media at day 14 (B) and 28 (C) ($n = 3$). For B and C, error bars represent mean ± SD and statistical significance was calculated using a one-way analysis of variance (ANOVA) with Tukey's multiple comparison test: n.s $p > 0.05$, (****) $p < 0.0001$, (***) $p < 0.001$, (**) $p < 0.01$, and (*) $p < 0.05$.

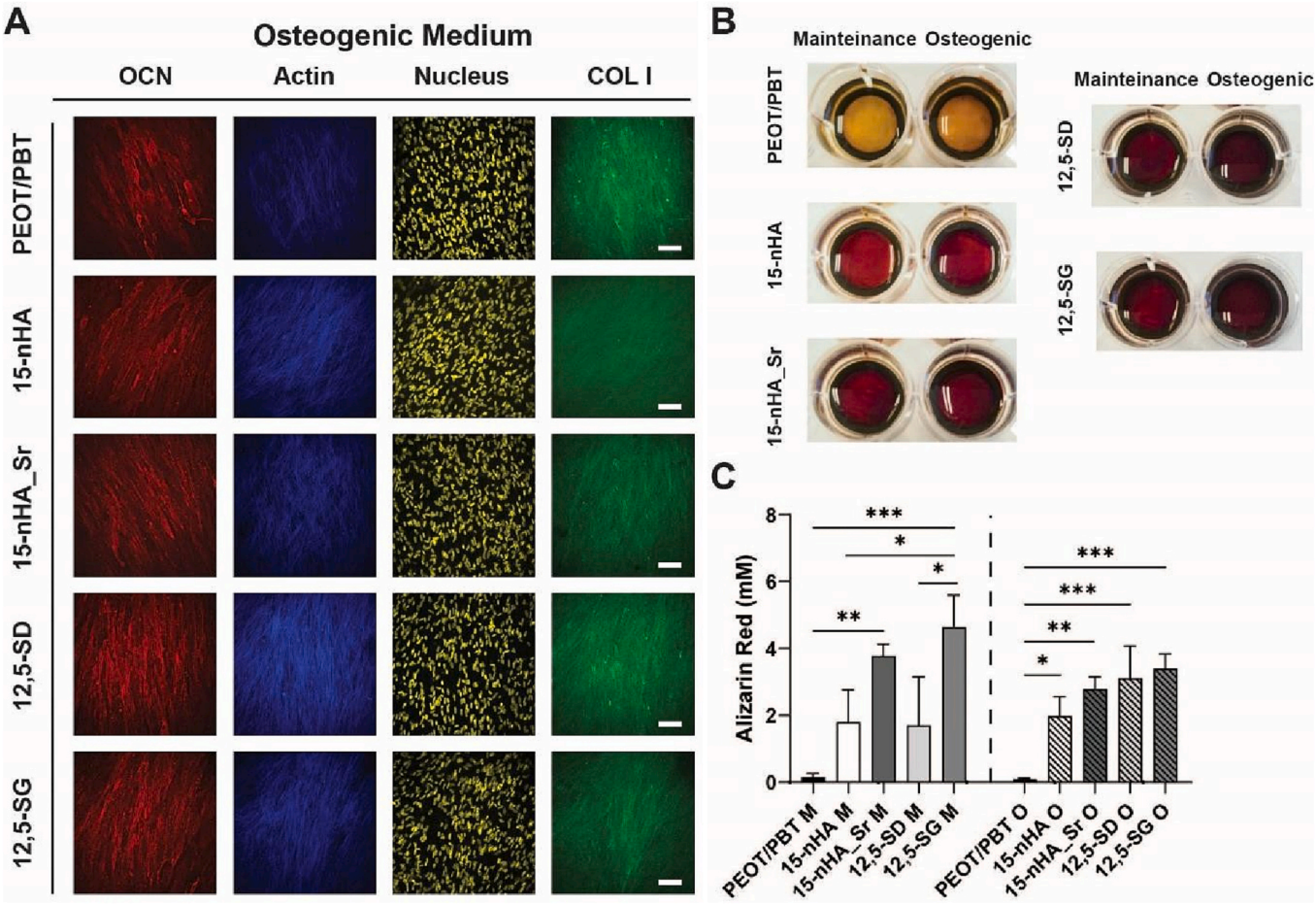

Fig. 7. Specialized matrix deposition on composite scaffolds. Representative confocal microscopy images of hMSCs cultured on the different composite and bare PEOT/PBT scaffolds stained for OCN (red), F-actin (blue), Cell nucleus (yellow) and COL1 (green) in osteogenic medium (A). Qualitative (B) and quantitative (C) Alizarin red staining at day 28 in maintenance and osteogenic media ($n = 3$). For C, error bars represent mean ± SD and statistical significance was calculated using a one-way analysis of variance (ANOVA) with Tukey's multiple comparison test: n.s $p > 0.05$, (****) $p < 0.0001$, (***) $p < 0.001$, (**) $p < 0.01$, and (*) $p < 0.05$. Scale bar in A is 100 μm.

In parallel, to assess ECM mineralization, alizarin red staining was performed at day 28 of culture. From macroscopic observation, it was clear that the red staining was more prominent in composite scaffolds (Fig. 7, B). However, it is well known that the ARS binds also to the calcium present in nHA and to MBGs [39]. Therefore, acellular composite scaffolds were used as a control (Fig. S10) and subtracted for quantification (Fig. 7, C). As shown in Fig. 7B, PEOT/PBT control had a low alizarin red concentration compared to 15-nHA_Sr and 12,5-SG in maintenance medium. In particular, 12,5-SG showed a concentration of 4,64 ± 0.95 mM, which was higher compared to 15-nHA and 12,5-SD with 1,79 ± 0,97 mM and 1,69 ± 1,46 mM, respectively. On the other hand, in osteogenic medium, alizarin red concentration of all composite scaffolds was higher with respect to the control, showing the positive effect of the incorporated particles to improve the deposition of calcium. Looking at the differentiation in 2D, it was observed that cells in maintenance medium had an alizarin red concentration of 0,22 ± 0,014 mM, which is lower compared to the composite scaffolds in the same medium. However, a higher concentration of 8,19 ± 0,66 mM was measured in osteogenic medium in 2D compared to scaffold culture.

3.6. Cell morphology and ECM deposition

At day 28, cell morphology and ECM deposition were imaged using SEM (Fig. S11). In all scaffolds, cells accounted for a spindle morphology, showing filopodia and lamellipodia, and were oriented in the same direction. The ECM appeared uniformly covering the surface of the scaffolds. These results demonstrated that not only cells adhered to the surface but also proliferated during the culture period on the scaffolds producing ECM. No particular difference in ECM was observed between hMSCs cultured in maintenance and osteogenic medium.

3.7. Gene expression

The gene expression of hMSCs cultured on electrospun scaffolds was analyzed at day 28 in maintenance and osteogenic media (Fig. 8). In maintenance medium (Fig. 8, A), hMSCs cultured on 15-nHA showed a similar gene expression profile compared to cells on the PEOT/PBT control. Moreover, COL1A1 and RUNX2 expression on 15-nHA were higher with respect to 15-nHA_Sr scaffolds. Interestingly, 15-nHA_Sr scaffolds showed a different expression profile with all the genes being downregulated compared to PEOT/PBT. In addition, the gene expression of RUNX2 and COL1A1 was also lower than all composite scaffolds, which in the case of COL1A1 could be correlated to a higher collagen secretion in the medium showed in Fig. 6. When analyzing the gene expression of hBMSCs cultured in the presence of MBGs containing scaffolds at day 35, it was noticed that the two kind of glasses induced a similar expression in the selected genes in maintenance medium as well as a similar expression profile compared to 15-nHA. Still, an upregulation of BMP2 was observed on 12,5-SD scaffolds which was not measured on 12,5-SG samples.

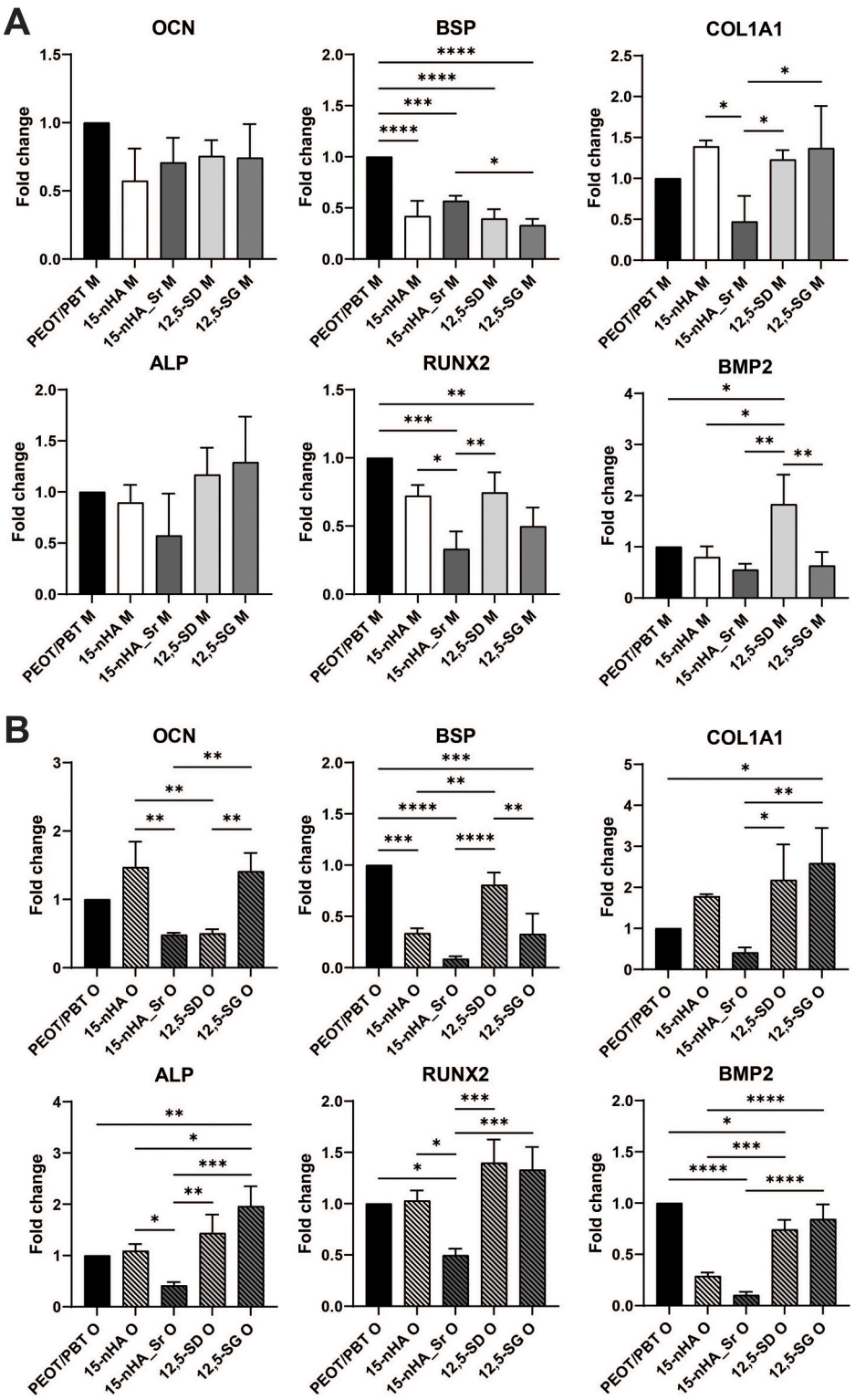

Fig. 8. Gene expression of hMSCs cultured on composite scaffolds at day 28 in maintenance medium (A) and osteogenic medium (B)($n = 3$). Error bars represent mean ± SD and statistical significance was calculated using a one-way analysis of variance (ANOVA) with Tukey's multiple comparison test: n.s $p > 0.05$, (****) $p < 0.0001$, (***) $p < 0.001$, (**) $p < 0.01$, and (*) $p < 0.05$.

In osteogenic medium, the gene expression of hBMSCs was analyzed for the same pool of genes by using PEOT/PBT scaffolds in osteogenic medium for normalization. The gene expression of OCN and COL1A1 was upregulated on 15-nHA scaffolds and following a similar trend as in maintenance medium. ALP and RUNX2 expression were comparable to PEOT/PBT but higher compared to 15-nHA_Sr. In addition, BSP and BMP2, markers of a mature bone ECM, were downregulated compared to the control. As for maintenance medium, 15-nHA_Sr scaffolds showed a downregulation in all genes compared to PEOT/PBT controls as well as lower than on 15-nHA scaffolds. On hMSCs cultured onto MBGs composite scaffolds, OCN expression of 12,5-SG was higher compared to 15-nHA_Sr and 12,5-SD, but comparable to PEOT/PBT. An opposite

response was observed in the expression of BSP, with 12,5-SD having a higher expression compared to 12,5-SG, which was downregulated compared to PEOT/PBT. Furthermore, for both MBGs there was an upregulation on the expression of COL1A1, ALP and RUNX2, in which 12,5-SD and 12,5-SG showed a higher expression compared to nHA-based scaffolds, with 12,5-SG having the highest fold change among the two MBGs composite scaffolds. Finally, BMP2 expression on 12,5-SG was comparable to PEOT/PBT scaffolds, whereas the gene expression of cells cultured on 12,5-SD was lower, but still higher as compared to cells cultured on 15-nHA scaffolds.

Interestingly, in the case of 2D cultures (Fig. S8, D), hMSC gene expression showed that OCN, BSP and COL1A1 were lower in osteogenic medium compared to maintenance medium while ALP, RUNX2 and BMP2 were higher. Therefore, to confirm hMSCs differentiation towards the osteogenic phenotype on the composites, scaffolds in osteogenic medium were compared to PEOT/PBT in maintenance medium. It was observed that BSP was higher in all scaffolds except for 15-nHA_Srx, while BMP2 was lower on nHA-based scaffolds compared to PEOT/PBT in maintenance medium. Still, RUNX2 showed an opposite trend for all scaffolds showing a lower expression in all conditions.

4. Discussion

Fabrication of Sr^{+2}-containing composite scaffolds by incorporation of inorganic phases into the electrospinning process is a promising strategy to develop scaffolds for bone tissue engineering applications. The aim of this work was to create composite scaffolds incorporating nHA, nHA_Sr and MBGs particles and evaluate in depth their morphological, chemical and mechanical properties alongside their biological performance. To obtain particle-loaded scaffolds, the preparation of the spinning solution is a key step. In order to get proper dispersion of the particles in the spinning solution, we showed that the sonication is beneficial, but the sonication time should be limited to 5 min to avoid damage of the inorganic phases and premature release of strontium (Fig. S1). Despite no change in the strontium concentration of MBGs after sonication and resuspension into the electrospinning solvent, a low decrease of about 5 % of the initial strontium content was recorded for nHA_Sr particles at the end of the process.

We were able to obtain composite scaffolds with up to 15 wt./vol% and 12,5 wt./vol% of nHA and MBGs into the polymeric PEOT/PBT scaffolds, respectively. Overall, composite scaffolds showed a smaller fiber diameter compared to PEOT/PBT scaffolds as well as a broader diameter range probably caused by partial embedding and aggregation of particles. In particular, 12,5-SG had a higher diameter compared to 12,5-SD. This is likely related to the particle dimensions. In fact, MBG_SG particles are in the nanometer range and tend to be embedded into the PEOT/PBT fibers while MBG_SD are bigger and tend to be segregated to the scaffold surface. For scaffold fabrication, higher particle concentrations were also attempted but led to needle clogging, thus compromising the fabrication process and defining the maximum quantity that could be incorporated into the system. However, even if high particle concentrations were ultimately used, particle agglomerates were uniformly spread throughout the meshes. In fact, Fig. 2 showed that aggregates of maximum 10 μm were present after electrospinning. This is in contrast to what has been reported in the literature [40,41], where larger particle agglomerates of up to 34,91 μm were observed on PCL/SrHA fibers when particle were dispersed in chloroform with the polymer. For MBGs, particle agglomerates were minimized to around 4–8 μm only when included in acetone (20 wt./vol%) and embedded at 5 wt% in PCL fibers [42]. Therefore, it was clear the efficacy of the sonication step to disperse the particles into the solution avoiding extensive agglomeration at high concentrations. To further improve particle distribution, particles could be sonicated for longer period of times with the final aim of acting as fillers in the electrospun scaffolds, reinforcing the mesh and increasing mechanical properties. However, this could ultimately lead to a decrease in the strontium content and damages to the particle morphology. Alternatively, particles could be modified (post-synthesis or *in situ* modification) to improve their dispersibility in the electrospinning solvent [43,44]. Currently, functionalization of particles has been mainly focusing on improve particles dispersibility in organic solvents [45], but could be applied in the future to electrospinning solvents such as isopropanol or chloroform. However, when looking at the fibers, only the surface was analyzed and not the entire scaffold. In fact, as observed in previous works [41,46], particle size influences their final distribution and location in the scaffolds. Smaller particles tend to become embedded into the fibers, limiting their availability. As expected, analysis of the fiber cross-section by TEM (Fig. S3) showed that nHA and nHA_Sr particles were also presented inside the PEOT/PBT fibers even at low nHA concentration. Moreover, the effective inclusion of the different inorganic particles on the composite scaffolds was further investigated by FTIR and EDX (Fig. 3). FTIR showed that the characteristic bands corresponding to the different particles were found into the composite scaffold spectra, while EDX analysis confirmed the inclusion of these by the elemental composition of the meshes. Once the scaffold composition was confirmed, their wettability was investigated to determine the effect of the particles on the surface properties (Supplementary Videos 1-5). Surface wettability has an important role in many biological processes [47] as the surface of a material is the first thing the cells come in contact with before having any cell to cell interaction [48]. Cell adhesive serum proteins such as fibronectin, fibrinogen, and vitronectin can modulate cell adhesion. Previous studies [49–51] have proven that hydrophilicity or hydrophobicity of the surface can facilitate the adherence of these proteins, thus affecting cell adhesion, proliferation and detachment. Independently of the formulation, scaffolds appeared to be hydrophilic, which is desirable for tissue engineering applications [52]. Similarly, previous works have already investigated the wettability of PEOT/PBT electrospun scaffolds, showing a contact angle of around 48–92,8° [34,53]. It is suggested that the porosity of the mesh plays a significant role on the absorption of the water drop onto the scaffold. In addition, HA and MBGs are well known to increase the wettability of electrospun scaffolds [54,55] by lowering the contact angle, thus improving cell-surface interactions.

Although our electrospun composite scaffolds are not fabricated for load-bearing purposes, the mechanical properties of a scaffold such as rigidity and elasticity should be investigated since they have a direct effect on their biological performance [56,57]. According to our measurements, the incorporation of particles into the mesh lowered the Young's modulus as well as the ultimate tensile strength. This trend is in line with data reported in previous works [58,59], where the incorporation of nHA and MBGs decreased the final material stiffness. It is proven that particles can maintain or improve the material stiffness when homogenized into the fabrication process [29,60]. This is likely an effect of the nanoparticles blending with the polymer into the fibers increasing their rigidity [61]. Therefore, this corroborates the higher Young modulus obtained for 15-nHA scaffolds, which are less compartmentalized compared to MBGs due to the distribution of nHA particles also into the fibers. However, when increasing the particle loading in the polymer matrix, particles start to agglomerate acting as defects, thus creating a less homogeneous mesh with stress concentration regions [58].

After studying the effect of the particles on the mechanical properties of the composite scaffolds, we also expected to note a dissimilarity in the strontium release curves from 15-nHA_Sr, 12,5-SD and 12,5-SG (Fig. 5). The release profile from 15-nHA_Sr showed a burst at 12 h, followed by a mild and steady release, slowly decreasing during the days. This is in line to what observed in previous works [28,62], where an initial burst release was correlated to the strontium ions coming from the particles on the surface of the scaffolds fibers, followed by a slow release from the nanofibers. In the 15-nHA_Sr scaffolds, the steady release of strontium probably derives from the nHA_Sr particles and aggregates exposed onto the fibers surface. Considering the presence of nHA_Sr observed in the

scaffolds cross sections, it is likely that the nanofibers would still be able to release Sr^{2+} for a prolonged amount of time due to the slow degradation time of PEOT/PBT [13]. Analysis of the Sr^{2+} release from MBGs-containing scaffolds was expected to exhibit a higher amount of Sr^{2+} being released compared to 15-nHA_Sr scaffolds as well as a burst release in the first days. As reported [63], the burst release is linked to the high surface of MBGs and to the particles size that improve ion diffusion through the porous structure.

In vitro, the optimal and most beneficial concentration of Sr^{2+} to induce osteogenic differentiation of hMSCs has still not been determined. Yet, investigating hMSC osteogenic differentiation onto nHA_Sr and MBGs-containing electrospun scaffolds, can give insight whether the strontium release from the particles can drive and improve the osteogenic differentiation in a long-term culture. Hence, cell attachment (Fig. 6, A) and proliferation (Fig. S7) were first evaluated. hMSCs showed a high cell attachment and viability on all PEOT/PBT-based composites, probably due to their hydrophilic nature and the enhanced protein adsorption coming from the particles [64,65]. In addition, cell number at day 7 showed no statistical difference between all the scaffolds tested. However, MBGs-loaded scaffolds presented a lower cell number compared to nHA-loaded and PEOT/PBT scaffolds. This result could be related to the high dose of strontium being released in the first days of culture in a suboptimal concentration to improve cell proliferation [66].

In vivo, different studies reported that the release of Sr^{2+} ions have also an effect on the matrix composition of the bone [67]. The bone matrix is rich in mostly collagen I and hydroxyapatite [68]. When in contact with cells, Sr^{2+} stimulates pre-osteoblasts and osteoblasts differentiation and proliferation increasing synthesis of collagen proteins [69] and matrix mineralization [27]. In this context, we analyzed the collagen secretion at day 14 and day 28 as well as the protein expression (collagen I and OCN) and the calcium deposits in the ECM at day 28. According to the data reported in Fig. 6B and C, the highest value of collagen secretion was found for hMSCs seeded onto 15-nHA_Sr scaffolds at day 14 in both maintenance and osteogenic media and also in maintenance medium at day 28. However at day 14 and 28, there was no statistical difference in collagen secretion between 15-nHA_Sr and 12,5-SD and 12,5-SG scaffolds in both media. These results corroborate the effect of the strontium on collagen synthesis in hMSCs. In addition, the highest secretion levels detected in 15-nHA_Sr could be associated to its steady Sr^{2+} release that maintains continuous stimulation on the cells during the long term culture [70]. Besides, by using the Sirius Red method, collagen III was detected alongside collagen I secretion. Collagen III has also been found into bone col1-containing fibrils and has been linked to osteoblastogenesis [71]. When protein expression was investigated, COL1 was expressed on electrospun scaffolds in maintenance and osteogenic media alongside OCN (Fig. 6, A). Interestingly, COL1 showed an intracellular expression on all scaffolds in maintenance medium (Fig. S9). This is possibly indicating that the Sr^{2+} release from the particles is capable of inducing an endogenous collagen synthesis even in the absence of ascorbic acid in the medium [72]. In addition, F-actin staining showed the presence of a great number of cells aligned on the scaffolds surface and embedded in the ECM. A confluent matrix layer was expected considering the results coming from Fig. S11, where PEOT/PBT-based scaffolds were completely covered by a dense ECM matrix. Consequently, we analyzed the ECM mineralized matrix by investigating the ARS staining at day 28 (Fig. 7, B and C). In maintenance medium, all composite scaffolds showed a higher ARS concentration compared to PEOT/PBT controls, further corroborating the beneficial effect of the particle on matrix mineralization also in a medium without osteogenic factors. 15-nHA_Sr and 12,5-SG scaffolds showed a moderately higher ARS concentration in maintenance medium compared to osteogenic medium. A possible explanation of the lower ARS levels seen in 12,5-SD could be the reduced cell number at day 7 before osteogenic induction. In fact, a lower density of cells can lead to a less mineralized matrix [73]. Contrary, all the other composite scaffolds had a similar ARS concentration in osteogenic medium, suggesting that the medium increased mineralization on 15-nHA and 12,5-SD scaffolds.

Osteogenic differentiation was also investigated through gene expression (Fig. 8). Bone markers for osteogenesis (OCN, BSP, COL1, ALP, RUNX2 and BMP2) were analyzed at day 28. Osteogenic genes such as OCN, BSP, and ALP are known to be influenced by strontium by the activation and phosphorylation of RUNX2 [74]. In maintenance medium, OCN, BSP, ALP and RUNX2 gene expression was not upregulated on composite scaffolds. This could be related to an early activation of RUNX2 in maintenance medium caused by the high release of strontium during the first days of culture [75]. However, in osteogenic medium ALP and RUNX2 expression in MBGs was upregulated, suggesting that in prolonged cultures, the medium might have a stronger effect than the particles. Contrarily, in osteogenic medium, 15-nHA showed a similar expression to PEOT/PBT in RUNX2 while resulted upregulated in OCN. These results are in line with literature [76], where a similar expression profile was also seen on 3D printed PEOT/PBT scaffolds loaded with nHA. Among all the conditions, 15-nHA_Sr was the only one that showed a downregulation in all genes. Yet, even if COL1 was downregulated, it was demonstrated that 15-nHA_Sr was the scaffold condition with the highest collagen secretion recorded with Sirius Red staining. Finally, among the bone morphogenic proteins, BMP2 plays an important role in hMSCs osteogenesis and matrix homeostasis and remodeling [77]. Among the scaffolds, 12,5-SD showed an upregulation of BMP2 in maintenance medium while gene expression of 12,5-SD and 12,5-SG was comparable to PEOT/PBT in osteogenic medium. Interestingly, in both media, RUNX2 and BMP2 showed similar expression profiles, possibly due to the BMP2 activation of RUNX2 [78].

Investigation of the biological performance of composite scaffolds revealed an effective osteogenic differentiation by the effect of the inorganic phase in conjunction with the strontium released from the meshes. However, while collagen secretion and matrix mineralization were enhanced on composite scaffolds, gene expression analysis showed that the expression of osteogenic markers was in many cases comparable or downregulated with respect to PEOT/PBT scaffolds, especially in the case of nHA_Sr-based scaffolds. Although it is not explicitly clear why strontium-containing scaffolds did not outperform PEOT/PBT controls at a gene level, MBG-loaded scaffolds still showed a higher osteogenic gene expression compared to nHA_Sr-loaded scaffolds in both media. To improve further the osteoinductivity of the strontium-containing scaffolds, the combination of nHA and MBGs by electrospinning could be explored to provide a controlled ion release. Alternatively, to avoid the embedding of nHA into the polymer fibers, the electrospraying technique could be employed to deposit the particles directly on the fiber surface [79], thus increasing the strontium release.

5. Conclusion

Through the addition of bioactive particles into PEOT/PBT, strontium-containing composite scaffolds were successfully fabricated by electrospinning. nHA and MBG particles were incorporated in the PEOT/PBT solution at relatively high concentrations. Overall, our results indicate that MBG particles could be included into the electrospinning process without damaging their morphology and preserving their strontium concentration while nHA_Sr particles showed a low decrease in the strontium content of around 5 %. All composite scaffolds showed a uniform distribution of particles with small aggregates, lower than 10 μm in size. The integration of particles led to a decrease in the fiber diameter and mechanical properties compared to neat PEOT/PBT meshes, but did not compromise the hydrophilicity of the scaffolds. In terms of ion release, strontium-containing particles showed two different Sr^{2+} release profiles, where MBGs-containing scaffolds tend to release most of the Sr^{2+} during the first week of culture while 15- nHA_Sr showed a short burst, followed by a slow release over 35 days. *In vitro* comparison between the different scaffold formulations showed that the inorganic phases enabled good hMSCs attachment and proliferation,

which were comparable to PEOT/PBT meshes after 1 week. However, during culture, the release of strontium from the composite scaffolds proved to induce higher collagen secretion compared to the PEOT/PBT and 15-nHA scaffolds in osteogenic medium. The inorganic phases also showed to increase mineralization on composite scaffolds and preserve the expression Col I and OCN in both maintenance and osteogenic media, directing osteogenic differentiation also in the absence of osteogenic factors. Most importantly, while 15-nHA_Sr provided better collagen secretion and matrix mineralization in both media, strontium-deficient 15-nHA had a higher expression of OCN, ALP and RUNX2 compared to 15-nHA_Sr scaffolds in osteogenic medium. Yet, MBG-loaded scaffolds expressed similar collagen secretion and matrix mineralization compared to 15-nHA_Sr, but their gene expression was higher in COL1, ALP, RUNX2 and BMP2 in osteogenic medium compared to nHA-based scaffolds, suggesting probably a more mature bone phenotype. Thus, MBGs- containing scaffolds could constitute a better candidate for bone applications.

In conclusion, our study on the collagen secretion, matrix deposition and mineralization, and gene expression provide a new insight on the osteogenic differentiation of hMSCs on 15-nHA, 15-nHA_Sr, 12,5-SD and 12,5-SG composite scaffolds. In this context, our data provides the basis for studies focusing on further combining strontium-containing nHA and MBGs through electrospinning to obtain a controlled ion release. Composite scaffolds could be used to deliver strontium as a bone-forming agent as well as an anti-osteoporotic treatment in case of pathological conditions.

Supplementary data to this article can be found online at https://doi.org/10.1016/j.bioadv.2023.213406.

CRediT authorship contribution statement

Clarissa Tomasina: Conceptualization, Methodology, Investigation, Writing – original draft, Formal analysis. **Giorgia Montalbano:** Investigation, Writing – review & editing, Formal analysis. **Sonia Fiorilli:** Writing – review & editing, Funding acquisition. **Paulo Quadros:** Writing – review & editing, Funding acquisition. **António Azevedo:** Writing – review & editing, Funding acquisition. **Catarina Coelho:** Writing – review & editing. **Chiara Vitale-Brovarone:** Conceptualization, Methodology, Writing – review & editing, Project administration, Funding acquisition. **Sandra Camarero-Espinosa:** Conceptualization, Methodology, Writing – review & editing, Supervision, Funding acquisition. **Lorenzo Moroni:** Conceptualization, Methodology, Writing – review & editing, Supervision, Project administration, Funding acquisition.

Declaration of competing interest

The authors declare that they have no known competing financial interests or personal relationships that could have appeared to influence the work reported in this paper.

Data availability

Data will be made available on request.

Acknowledgements

The authors thank the M4i institute of Maastricht University for their support with the confocal imaging and the transmission electron microscopy.

This project has received funding from the European Union's Horizon 2020 research and innovation program under grant agreement No. 814410.

References

[1] A.R. Amini, C.T. Laurencin, S.P. Nukavarapu, Bone tissue engineering: recent advances and challenges, Crit. Rev. Biomed. Eng. 40 (5) (2012) 363–408.
[2] G. Tang, Z. Liu, Y. Liu, J. Yu, X. Wang, Z. Tan, X. Ye, Recent trends in the development of bone regenerative biomaterials, Fronti. Cell Dev. Biol. 9 (2021).
[3] F.R.A.J. Rose, R.O.C. Oreffo, Bone tissue engineering: hope vs hype, Biochem. Biophys. Res. Commun. 292 (1) (2002) 1–7.
[4] D.-L. Yang, F. Faraz, J.-X. Wang, N. Radacsi, Combination of 3D printing and electrospinning techniques for biofabrication, Adv. Mater. Technol. 7 (7) (2022) 2101309.
[5] W.E. Teo, S. Ramakrishna, A review on electrospinning design and nanofibre assemblies, Nanotechnology 17 (14) (2006) R89.
[6] S. Anjum, F. Rahman, P. Pandey, D.K. Arya, M. Alam, P.S. Rajinikanth, Q. Ao, Electrospun biomimetic nanofibrous scaffolds: a promising Prospect for bone tissue engineering and regenerative medicine, Int. J. Mol. Sci. 23 (16) (2022) 9206.
[7] K. Zhang, Y. Fan, N. Dunne, X. Li, Effect of microporosity on scaffolds for bone tissue engineering, Regen. Biomater. 5 (2) (2018) 115–124.
[8] L.S.C.G.Petre Daniela Geta, The use of fibers in bone tissue engineering, Tissue Eng. Part B Rev. 28 (1) (2022) 141–159.
[9] M. Keshvardoostchokami, S.S. Majidi, P. Huo, R. Ramachandran, M. Chen, B. Liu, Electrospun nanofibers of natural and synthetic polymers as artificial extracellular matrix for tissue engineering, Nanomaterials (Basel) 11 (1) (2020).
[10] A. Nandakumar, H. Fernandes, J. de Boer, L. Moroni, P. Habibovic, C.A. van Blitterswijk, Fabrication of bioactive composite scaffolds by electrospinning for bone regeneration, Macromol. Biosci. 10 (11) (2010) 1365–1373.
[11] T.B. Woodfield, J. Malda, J. de Wijn, F. Péters, J. Riesle, C.A. van Blitterswijk, Design of porous scaffolds for cartilage tissue engineering using a three-dimensional fiber-deposition technique, Biomaterials 25 (18) (2004) 4149–4161.
[12] A.M. Radder, J.E. Davies, H. Leenders, C.A. van Blitterswijk, Interfacial behavior of PEO/PBT copolymers (Polyactive) in a calvarial system: an in vitro study, J. Biomed. Mater. Res. 28 (2) (1994) 269–277.
[13] A.A. Deschamps, A.A. van Apeldoorn, H. Hayen, J.D. de Bruijn, U. Karst, D. W. Grijpma, J. Feijen, In vivo and in vitro degradation of poly(ether ester) block copolymers based on poly(ethylene glycol) and poly(butylene terephthalate), Biomaterials 25 (2) (2004) 247–258.
[14] E. Ewaldz, B. Brettmann, Molecular interactions in electrospinning: from polymer mixtures to supramolecular assemblies, ACS Appl. Polym. Mater. 1 (3) (2019) 298–308.
[15] M.M. Stevens, J.H. George, Exploring and engineering the cell surface interface, Science 310 (5751) (2005) 1135–1138.
[16] H. Zhou, J. Lee, Nanoscale hydroxyapatite particles for bone tissue engineering, Acta Biomater. 7 (7) (2011) 2769–2781.
[17] B. Liang, T. Feng, X. Yuan, K. Zhao, C. Li, Y. Han, Proportion-dependent osteogenic activity of electrospun nano-hydroxyapatite/polylactic acid fiber membrane in vitro and in vivo, Mater. Des. 219 (2022), 110834.
[18] H. Li, C. Huang, X. Jin, Q. Ke, An electrospun poly(ε-caprolactone) nanocomposite fibrous mat with a high content of hydroxyapatite to promote cell infiltration, RSC Adv. 8 (44) (2018) 25228–25235.
[19] B. Safari, A. Aghanejad, L. Roshangar, S. Davaran, Osteogenic effects of the bioactive small molecules and minerals in the scaffold-based bone tissue engineering, Colloids Surf. B: Biointerfaces 198 (2021), 111462.
[20] C. Wu, J. Chang, Mesoporous bioactive glasses: structure characteristics, drug/growth factor delivery and bone regeneration application, Interface Focus 2 (3) (2012) 292–306.
[21] X. Zhang, D. Zeng, N. Li, J. Wen, X. Jiang, C. Liu, Y. Li, Functionalized mesoporous bioactive glass scaffolds for enhanced bone tissue regeneration, Sci. Rep. 6 (1) (2016) 19361.
[22] J. Li, C. Wang, G. Gao, X. Yin, X. Pu, B. Shi, Y. Liu, Z. Huang, J. Wang, J. Li, G. Yin, MBG/ PGA-PCL composite scaffolds provide highly tunable degradation and osteogenic features, Bioactive Materials 15 (2022) 53–67.
[23] D. Zeng, X. Zhang, X. Wang, Q. Huang, J. Wen, X. Miao, L. Peng, Y. Li, X. Jiang, The osteoimmunomodulatory properties of MBG scaffold coated with amino functional groups, Artif. Cells Nanomed. Biotechnol. 46 (7) (2018) 1425–1435.
[24] Z. Neščáková, K. Zheng, L. Liverani, Q. Nawaz, D. Galusková, H. Kaňková, M. Michálek, D. Galusek, A.R. Boccaccini, Multifunctional zinc ion doped sol - gel derived mesoporous bioactive glass nanoparticles for biomedical applications, Bioact Mater 4 (2019) 312–321.
[25] A. Bari, N. Bloise, S. Fiorilli, G. Novajra, M. Vallet-Regí, G. Bruni, A. Torres-Pardo, J.M. González-Calbet, L. Visai, C. Vitale-Brovarone, Copper-containing mesoporous bioactive glass nanoparticles as multifunctional agent for bone regeneration, Acta Biomater. 55 (2017) 493–504.
[26] A. Hoppe, V. Mouriño, A.R. Boccaccini, Therapeutic inorganic ions in bioactive glasses to enhance bone formation and beyond, Biomaterials Science 1 (3) (2013) 254–256.
[27] B. Kołodziejska, N. Stępień, J. Kolmas, The influence of strontium on bone tissue metabolism and its application in osteoporosis treatment, Int. J. Mol. Sci. 22 (12) (2021).
[28] H. Ye, J. Zhu, D. Deng, S. Jin, J. Li, Y. Man, Enhanced osteogenesis and angiogenesis by PCL/chitosan/Sr-doped calcium phosphate electrospun nanocomposite membrane for guided bone regeneration, J. Biomater. Sci. Polym. Ed. 30 (16) (2019) 1505–1522.
[29] J.S. Fernandes, P. Gentile, M. Martins, N.M. Neves, C. Miller, A. Crawford, R. A. Pires, P. Hatton, R.L. Reis, Reinforcement of poly-l-lactic acid electrospun membranes with strontium borosilicate bioactive glasses for bone tissue engineering, Acta Biomater. 44 (2016) 168–177.

[30] V.M.T.M. Silva, P.A. Quadros, P.E.M.S.C. Laranjeira, M.M. Dias, J.C.B. Lopes, A novel continuous industrial process for producing hydroxyapatite nanoparticles, J. Dispers. Sci. Technol. 29 (4) (2008) 542–547.
[31] L.P.Lopes JC, M.M. Dias, A.A. Martins, in: O. WIP (Ed.), Network Mixer and Related Mixing Process, 2005.
[32] S. Fiorilli, M. Pagani, E. Boggio, C.L. Gigliotti, C. Dianzani, R. Gauthier, C. Pontremoli, G. Montalbano, U. Dianzani, C. Vitale-Brovarone, Sr-containing mesoporous bioactive glasses bio-functionalized with recombinant ICOS-Fc: an in vitro study, Nanomaterials (Basel) 11 (2) (2021) 321.
[33] A. Georgopoulou, M. Kaliva, M. Vamvakaki, M. Chatzinikolaidou, Osteogenic potential of pre-osteoblastic cells on a chitosan-graft-polycaprolactone copolymer, Materials (Basel, Switzerland) 11 (4) (2018) 490.
[34] A.F. Girão, P. Wieringa, S.C. Pinto, P.A.A.P. Marques, S. Micera, R. van Wezel, M. Ahmed, R. Truckenmueller, L. Moroni, Ultraviolet functionalization of electrospun scaffolds to activate fibrous runways for targeting cell adhesion, Front. Bioeng. Biotechnol. (2019) 159.
[35] N. Ribeiro, S.R. Sousa, C.A. van Blitterswijk, L. Moroni, F.J. Monteiro, A biocomposite of collagen nanofibers and nanohydroxyapatite for bone regeneration, Biofabrication 6 (3) (2014), 035015.
[36] J. Jeong, J.H. Kim, J.H. Shim, N.S. Hwang, C.Y. Heo, Bioactive calcium phosphate materials and applications in bone regeneration, Biomaterials Research 23 (1) (2019) 4.
[37] A.L. Rossi, S. Moldovan, W. Querido, A. Rossi, J. Werckmann, O. Ersen, M. Farina, Effect of strontium ranelate on bone mineral: analysis of nanoscale compositional changes, Micron 56 (2014) 29–36.
[38] E.F. Morgan, G.U. Unnikrisnan, A.I. Hussein, Bone mechanical properties in healthy and diseased states, Annu. Rev. Biomed. Eng. 20 (2018) 119–143.
[39] H.M. Myers, Orientation of adsorbed alizarin red S on hydroxyapatite, Calcif. Tissue Int. 34 (Suppl 2) (1982) S57–S61.
[40] E.V. Melnik, S.N. Shkarina, S.I. Ivlev, V. Weinhardt, T. Baumbach, M.V. Chaikina, M.A. Surmeneva, R.A. Surmenev, In vitro degradation behaviour of hybrid electrospun scaffolds of polycaprolactone and strontium-containing hydroxyapatite microparticles, Polym. Degrad. Stab. 167 (2019) 21–32.
[41] I. Rajzer, M. Dziadek, A. Kurowska, K. Cholewa-Kowalska, M. Ziąbka, E. Menaszek, T.E.L. Douglas, Electrospun polycaprolactone membranes with zn-doped bioglass for nasal tissues treatment, J. Mater. Sci. Mater. Med. 30 (7) (2019) 80.
[42] R. Sergi, V. Cannillo, A.R. Boccaccini, L. Liverani, Incorporation of bioactive glasses containing mg, sr, and zn in electrospun PCL fibers by using benign solvents, Appl. Sci. 10 (16) (2020) 5530.
[43] H. Kamiya, M. Iijima, Surface modification and characterization for dispersion stability of inorganic nanometer-scaled particles in liquid media, Sci. Technol. Adv. Mater. 11 (4) (2010), 044304.
[44] V. Stanić, Variation in properties of bioactive glasses after surface modification, in: Clinical Applications of Biomaterials: State-of-the-Art Progress, Trends, and Novel Approaches, 2017, pp. 35–63.
[45] V. González-Rodríguez, D. Lizeth Zapata-Tello, J. Vallejo-Montesinos, R. Zárraga Núñez, J. Amir Gonzalez-Calderon, E. Pérez, Improving titanium dioxide dispersion in water through surface functionalization by a dicarboxylic acid, J. Dispers. Sci. Technol. 40 (7) (2019) 1039–1045.
[46] A. Patlolla, G. Collins, T. Livingston Arinzeh, Solvent-dependent properties of electrospun fibrous composites for bone tissue regeneration, Acta Biomater. 6 (1) (2010) 90–101.
[47] T. Huhtamäki, X. Tian, J.T. Korhonen, R.H.A. Ras, Surface-wetting characterization using contact-angle measurements, Nat. Protoc. 13 (7) (2018) 1521–1538.
[48] K.L. Menzies, L. Jones, The impact of contact angle on the biocompatibility of biomaterials, Optom. Vis. Sci. 87 (6) (2010).
[49] Y. Arima, H. Iwata, Effect of wettability and surface functional groups on protein adsorption and cell adhesion using well-defined mixed self-assembled monolayers, Biomaterials 28 (20) (2007) 3074–3082.
[50] R. Tzoneva, N. Faucheux, T. Groth, Wettability of substrata controls cell-substrate and cell-cell adhesions, Biochim. Biophys. Acta 1770 (11) (2007) 1538–1547.
[51] J. Bae, K.S. Kim, H. Choi, H. Kim, Effect of asymmetric wettability in nanofiber membrane by electrospinning technique on separation of oil/water emulsion, Chemosphere 204 (2018) 235–242.
[52] B. Niemczyk-Soczynska, A. Gradys, P. Sajkiewicz, Hydrophilic surface functionalization of electrospun nanofibrous scaffolds in tissue engineering, Polymers (Basel) 12 (11) (2020).
[53] H. Chen, X. Huang, M. Zhang, F. Damanik, M.B. Baker, A. Leferink, H. Yuan, R. Truckenmüller, C. van Blitterswijk, L. Moroni, Tailoring surface nanoroughness of electrospun scaffolds for skeletal tissue engineering, Acta Biomater. 59 (2017) 82–93.
[54] R.A. Surmenev, S. Shkarina, D.S. Syromotina, E.V. Melnik, R. Shkarin, I. I. Selezneva, A.M. Ermakov, S.I. Ivlev, A. Cecilia, V. Weinhardt, T. Baumbach, T. Rijavec, A. Lapanje, M.V. Chaikina, M.A. Surmeneva, Characterization of biomimetic silicate- and strontium-containing hydroxyapatite microparticles embedded in biodegradable electrospun polycaprolactone scaffolds for bone regeneration, Eur. Polym. J. 113 (2019) 67–77.
[55] Z. Tabia, S. Akhtach, M. Bricha, K. El Mabrouk, Tailoring the biodegradability and bioactivity of green-electrospun polycaprolactone fibers by incorporation of bioactive glass nanoparticles for guided bone regeneration, Eur. Polym. J. 161 (2021), 110841.
[56] D.E. Discher, P. Janmey, Y.-L. Wang, Tissue cells feel and respond to the stiffness of their substrate, Science 310 (5751) (2005) 1139–1143.
[57] B.P. Chan, K.W. Leong, Scaffolding in tissue engineering: general approaches and tissue-specific considerations, Eur Spine J 17 (Suppl 4) (2008) 467–479.
[58] D. Moura, M.T. Souza, L. Liverani, G. Rella, G.M. Luz, J.F. Mano, A.R. Boccaccini, Development of a bioactive glass-polymer composite for wound healing applications, Mater. Sci. Eng. C 76 (2017) 224–232.
[59] M.K. Ahmed, S.F. Mansour, R. Al-Wafi, E. Abdel-Fattah, Nanofibers scaffolds of co-doped Bi/Sr-hydroxyapatite encapsulated into polycaprolactone for biomedical applications, J. Mater. Res. Technol. 13 (2021) 2297–2309.
[60] J.-H. Jo, E.-J. Lee, D.-S. Shin, H.-E. Kim, H.-W. Kim, Y.-H. Koh, J.-H. Jang, In vitro/in vivo biocompatibility and mechanical properties of bioactive glass nanofiber and poly(ε-caprolactone) composite materials, J. Biomed. Mater. Res. B Appl. Biomater. 91B (1) (2009) 213–220.
[61] A. Kausar, Polymeric nanocomposite via electrospinning: assessment of morphology, physical properties and applications, J. Plastic Film Sheet. 37 (1) (2021) 70–92.
[62] J. Hao, A. Acharya, K. Chen, J. Chou, S. Kasugai, N.P. Lang, Novel bioresorbable strontium hydroxyapatite membrane for guided bone regeneration, Clin. Oral Implants Res. 26 (1) (2015) 1–7.
[63] S. Fiorilli, G. Molino, C. Pontremoli, G. Iviglia, E. Torre, C. Cassinelli, M. Morra, C. Vitale-Brovarone, The incorporation of strontium to improve bone-regeneration ability of mesoporous bioactive glasses, Materials 11 (5) (2018) 678.
[64] C. Wu, W. Fan, M. Gelinsky, Y. Xiao, P. Simon, R. Schulze, T. Doert, Y. Luo, G. Cuniberti, Bioactive SrO–SiO2 glass with well-ordered mesopores: characterization, physiochemistry and biological properties, Acta Biomater. 7 (4) (2011) 1797–1806.
[65] T. Lan, Z.-Q. Shao, J.-Q. Wang, M.-J. Gu, Fabrication of hydroxyapatite nanoparticles decorated cellulose triacetate nanofibers for protein adsorption by coaxial electrospinning, Chem. Eng. J. 260 (2015) 818–825.
[66] M. Schumacher, A. Lode, A. Helth, M. Gelinsky, A novel strontium(II)-modified calcium phosphate bone cement stimulates human-bone-marrow-derived mesenchymal stem cell proliferation and osteogenic differentiation in vitro, Acta Biomater. 9 (12) (2013) 9547–9557.
[67] W. Querido, A.L. Rossi, M. Farina, The effects of strontium on bone mineral: a review on current knowledge and microanalytical approaches, Micron 80 (2016) 122–134.
[68] A.L. Boskey, Bone composition: relationship to bone fragility and antiosteoporotic drug effects, Bonekey Rep 2 (2013) 447.
[69] M.M. Almeida, E.P. Nani, L.N. Teixeira, D.C. Peruzzo, J.C. Joly, M.H. Napimoga, E. F. Martinez, Strontium ranelate increases osteoblast activity, Tissue Cell 48 (3) (2016) 183–188.
[70] E. Boanini, P. Torricelli, M. Fini, A. Bigi, Osteopenic bone cell response to strontium-substituted hydroxyapatite, J. Mater. Sci. Mater. Med. 22 (9) (2011) 2079–2088.
[71] S.W. Volk, S.R. Shah, A.J. Cohen, Y. Wang, B.K. Brisson, L.K. Vogel, K. D. Hankenson, S.L. Adams, Type III collagen regulates osteoblastogenesis and the quantity of trabecular bone, Calcif. Tissue Int. 94 (6) (2014) 621–631.
[72] Endogenous collagen influences differentiation of human multipotent mesenchymal stromal cells, Tissue Engineering Part A 16 (5) (2010).
[73] C.E. Holy, M.S. Shoichet, J.E. Davies, Engineering three-dimensional bone tissue in vitro using biodegradable scaffolds: investigating initial cell-seeding density and culture period, J. Biomed. Mater. Res. 51 (3) (2000) 376–382.
[74] D. Marx, A. Rahimnejad Yazdi, M. Papini, M. Towler, A review of the latest insights into the mechanism of action of strontium in bone, Bone Rep. 12 (2020), 100273.
[75] Y. Li, C. Ge, J.P. Long, D.L. Begun, J.A. Rodriguez, S.A. Goldstein, R.T. Franceschi, Biomechanical stimulation of osteoblast gene expression requires phosphorylation of the RUNX2 transcription factor, J. Bone Miner. Res. 27 (6) (2012) 1263–1274.
[76] M. Cámara-Torres, R. Sinha, A. Sanchez, P. Habibovic, A. Patelli, C. Mota, L. Moroni, Effect of Highly Loaded Nanohydroxyapatite Composite Scaffolds Prepared via Melt Extrusion Additive Manufacturing on the Osteogenic Differentiation of Human Mesenchymal Stromal Cells, bioRxiv, 2021, 2021.01.21.427568.
[77] H. Cai, J. Zou, W. Wang, A. Yang, BMP2 induces hMSC osteogenesis and matrix remodeling, Mol. Med. Rep. 23 (2) (2021).
[78] V. Rosen, BMP2 signaling in bone development and repair, Cytokine Growth Factor Rev. 20 (5–6) (2009) 475–480.
[79] C. Gandhimathi, J.R. Venugopal, S. Ramakrishna, D.K. Srinivasan, Electrospun-electrosprayed hydroxyapatite nanostructured composites for bone tissue regeneration, J. Appl. Polym. Sci. 135 (42) (2018) 46756.